Published in final edited form as:
Gene Expr Patterns. 2013 October ; 13(7): 225–239. doi:10.1016/j.gep.2013.04.003.

Widespread but tissue-specific patterns of interferon-induced transmembrane protein 3 (IFITM3, FRAGILIS, MIL-1) in the mouse gastrula

Maria M. Mikedis and **Karen M. Downs***
Department of Cell and Regenerative Biology University of Wisconsin-Madison School of Medicine and Public Health 1300 University Avenue Madison, WI 53706

Abstract

Interferon-induced transmembrane protein 3 (IFITM3; FRAGILIS; MIL-1) is part of a larger family of important small interferon-induced transmembrane genes and proteins involved in early development, cell adhesion, and cell proliferation, and which also play a major role in response to bacterial and viral infections and, more recently, in pronounced malignancies (Siegrist et al., 2011). IFITM3, together with tissue-nonspecific alkaline phosphatase (TNAP), PRDM1, and STELLA, has been claimed to be a hallmark of segregated primordial germ cells (PGCs) (Saitou et al., 2002). However, whether IFITM3, like STELLA, is part of a broader stem/progenitor pool that builds the posterior region of the mouse conceptus (Mikedis and Downs, 2012), is obscure. To discover the whereabouts of IFITM3 during mouse gastrulation (~E6.5-9.0), systematic immunohistochemical analysis was carried out at closely spaced 2-4-hour intervals. Results revealed diverse, yet consistent, profiles of IFITM3 localization throughout the gastrula. Within the putative PGC trajectory and surrounding posterior tissues, IFITM3 localized as a large cytoplasmic spot with or without staining in the plasma membrane. IFITM3, like STELLA, was also found in the ventral ectodermal ridge (VER), a posterior progenitor pool that builds the tailbud. The large cytoplasmic spot with plasma membrane staining was exclusive to the posterior region; the visceral yolk sac, non-posterior tissues, and epithelial tissues exhibited spots of IFITM3 without cell surface staining. Co-localization of the intracellular IFITM3 spot with the endoplasmic reticulum, Golgi apparatus or endolysosomes was not observed. That relatively high levels of IFITM3 were found throughout the posterior primitive streak and its derivatives is consistent with evidence that IFITM3, like STELLA, is part of a larger stem/progenitor cell pool at the posterior end of the primitive streak that forms the base of the allantois and builds the fetal-umbilical connection, thus further obfuscating practical phenotypic distinctions between so-called PGCs and surrounding soma.

Keywords

Allantoic Core Domain; allantois; branchial arches; IFITM2; IFITM3; endothelium; *Flk1*; foregut; FRAGILIS; hematopoietic cells; hindgut; MIL-1; mouse; primitive streak; primordial germ cells; PGCs; *Runx1*; ventral ectodermal ridge

*Author for correspondence: Tel: 608-265-5411 Fax: 608-262-7306 kdowns@wisc.edu.

1. INTRODUCTION

A variety of cell lineages are formed in the posterior region of the mouse conceptus, yet only the primordial germ cells (PGCs) have undergone long-standing scrutiny there (reviewed in Hayashi et al., 2007; McLaren, 2000). Over the past decade, efforts have intensified to identify genes that regulate the segregation of PGCs from surrounding soma. The current view is that PGC progenitors arise in proximal epiblast, and express PR domain zinc finger protein 1 (*Prdm1*; also *Blimp1*) (Ohinata et al., 2005) as well as interferon-induced transmembrane protein 3 (*Ifitm3*; also *Fragilis, Mil*-1) (Lange et al., 2003; Saitou et al., 2002; Tanaka and Matsui, 2002), making them distinct from surrounding soma. *Prdm1/Ifitm3*-expressing epiblast cells then move into the primitive streak, from which they translocate with streak mesoderm into the base of the allantois and begin to co-express tissue non-specific alkaline phosphatase (TNAP; Lawson and Hage, 1994) and *Stella* (*Dppa3, PGC7*). Thus, a small cluster of *Prdm1/Ifitm3*/TNAP*/Stella*-positive PGCs (Ohinata et al., 2005; Saitou et al., 2002) is located within the midline of the base of the allantois. However, none of these PGC hallmark gene products, if absent, has demonstrated effects on fertility (Bortvin et al., 2004; Lange et al., 2008; Macgregor et al., 1995; Payer et al., 2003; Vincent et al., 2005).

Alkaline phosphatase (AP) activity (Benham et al., 1983; Bernstine et al., 1973) and STELLA (Bowles et al., 2003; Carter et al., 2008) are individually associated with pluripotency, while PRDM1 (Horsley et al., 2006; Mould et al., 2012; Nishikawa et al., 2010; Turner et al., 1994) and AP activity (Jaiswal et al., 1997; Lewinson et al., 1982) have each been associated with progenitor cell populations. All of these gene products are found within a self-propagating stable stem/progenitor cell population in the base of the allantois, called the Allantoic Core Domain (ACD; Downs et al., 2009). In eutherian mammals, the allantois is the source of the umbilical cord which, through connection to the fetus and yolk sac, ensures a vascular continuum throughout the conceptus.

Intriguingly, DiI fate mapping the ACD has revealed that it is both a self-propagating midline population, similar to the node at the anterior end of the streak (Beddington, 1994), and a source of the distal region of the allantois (Downs et al., 2009). In the absence of the ACD, the allantois fails to elongate and vascularize (Downs et al., 2009; Inman and Downs, 2006).

Following the discovery of the ACD, we re-investigated the whereabouts of STELLA. Careful spatiotemporal histological analysis at closely-spaced intervals and fate mapping demonstrated that, from the precursor ACD, STELLA spreads to the intraembryonic primitive streak (IPS); both the ACD and IPS make overlapping and distinct STELLA-positive contributions to the fetal-umbilical connection (Mikedis and Downs, 2012), including the allantois, ventral hindgut, posterior mesoderm, and ventral ectodermal ridge (VER). Thus, STELLA is not restricted to the putative germ line but is part of a broader pool of posterior primitive streak stem/progenitor cells that build the posterior region of the eutherian mammal, ensuring proper development of the fetal-umbilical connection. These results beg the question of what is and is not a primordial germ cell.

Here we now report the whereabouts of IFITM3, beginning just prior to formation of the primitive streak and through elaboration of the hindgut (~E6.5-9.0). All other tissues within the mouse gastrula were analyzed, and localization of IFITM3 to them is also reported. We have found that IFITM3 localization as a cytoplasmic spot with cell surface staining, previously associated with the putative PGCs (Saitou et al., 2002), is unique to the posterior region but is not restricted to the putative PGC trajectory. Additional IFITM3, primarily as a cytoplasmic spot without cell surface staining, was localized throughout the conceptus.

2. RESULTS

2.1. Specificity of IFITM3 antibody

The commercially available antibody used to identify IFITM3 was raised against a synthetic peptide derived from within the first 50 residues of the mouse IFITM3 N-terminal region. To preliminarily confirm antibody specificity, we used the NCBI BLAST database (http://blast.ncbi.nlm.nih.gov/Blast.cgi) to identify mouse proteins that share sequence similarity to this synthetic peptide sequence (proprietary information; contact technical support at Abcam for further details). The only protein with sequence similarity to the IFITM3 synthetic peptide was family member IFITM2 ($E<0.01$). For all other protein matches, $E>0.01$; thus, no other proteins exhibited significant sequence similarity to the synthetic peptide.

As IFITM2 and IFITM3 have predicted molecular weights (MW) of 15.7 kDa and 15.0 kDa (UniProtKB), respectively, they cannot be reliably distinguished as distinct bands on a Western blot. Nor can immunohistochemical methods be used to determine whether the antibody exclusively identifies IFITM3, as *Ifitm2* and *Ifitm3* are expressed in similar tissues in the mouse conceptus (Lange et al., 2003). Therefore, to test whether anti-IFITM3 detects IFITM2, our overall plan was to carry out Western blotting on mouse IFITM2-transfected 293T protein extract, using IFITM2-negative 293T cells as a negative control and mouse embryonic fibroblast NIH 3T3 cells as a positive control for the presence of IFITM3 (Bailey et al., 2012; Brass et al., 2009).

We first verified the presence of IFITM2 in IFITM2-transfected 293T cell lysate using an antibody that detects both IFITM2 and IFITM3 (anti-IFITM2/3); IFITM3-positive mouse embryonic fibroblast NIH 3T3 cell lysate was used as a positive control. Anti-IFITM2/3 detected a protein band at ~15.0 in IFITM2:293T lysate (**Fig. 1A$_1$**, lane 2) and NIH 3T3 lysate (**Fig. 1A$_1$**, lane 4), but did not identify any bands in the negative control, 293T lysate (**Fig. 1A$_1$**, lane 3). By contrast, anti-IFITM3 did not detect IFITM2 in the IFITM2:293T lysate (**Fig. 1A$_1$**, lane 5, below asterisk) or negative control, 293T lysate (**Fig. 1A$_1$, lane 6)**, but did detect it in the positive control, NIH 3T3 lysate (**Fig. 1A$_1$, lane 7**). Although anti-IFITM3 detected higher molecular weight protein bands in IFITM2:293T lysate at ~31.0 and ~66.0 kDa (**Fig. 1 A$_1$**, lane 5), these bands were also present in IFITM2-negative 293T lysate (**Fig. 1 A$_1$**, lane 6). Therefore, despite the sequence similarity between IFITM2 and the immunogen used to produce anti-IFITM3, the IFITM3 antibody does not identify IFITM2.

We then confirmed anti-IFITM3 specificity in mouse conceptuses by Western blot analysis of total protein at combined EHF-6-s stages (~E7.75-8.5), when our preliminary experiments revealed that IFITM3 was present. Four reactions were carried out: (i) fresh primary antibody (**Fig. 1A$_2$**, lanes 9, 10 and **Fig. 1A$_3$**, lanes 14, 15 representing two biological replicates for both the embryonic cell lysate and the IFITM3-positive NIH 3T3 cell lysate); (ii) elimination of the primary anti-IFITM3 (**Fig. 1A$_2$**, lanes 11, 12); (iii) pre-binding primary anti-IFITM3 alone with its cognate control peptide sequence for 1 hour at room temperature (**Fig. 1A$_3$**, lanes 16, 17); and (iv) primary anti-IFITM3 alone, incubated for 1 hour at room temperature (**Fig. 1A$_3$**, lanes 18, 19). In the embryonic and IFITM3-positive NIH 3T3 lysates, fresh anti-IFITM3 identified one band slightly above the 14.4 kDa molecular weight mark that is consistent with IFITM3's predicted MW of 15.0 kDa (**Fig. 1A$_2$**, lanes 2-3; **Fig. 1A$_3$**, lanes 14, 15). In addition, the IFITM3-positive NIH 3T3 cell lysates had an additional band just below the 14.4 kDa molecular weight mark (**Fig. 1A$_1$**, lanes 7; **Fig. 1A$_2$**, lane 10; **Fig. 1A$_3$**, lane 15), which may represent a degradation product of IFITM3. The Western blot analysis also revealed one (total embryonic lysate) or three (IFITM3-positive NIH 3T3 lysate) bands above the predicted 15.0 kDa that appeared to be approximate multiples of 15 kDa (**Fig. 1A$_3$, lanes 14, 15**); these are consistent with

polyubiquitination of IFITM3 at up to four lysine residues (Yount et al., 2012). As the MW of ubiquitin is 8.5 kDa (reviewed in Hasselgren and Fischer, 1997), the approximately 15.0 kDa intervals between IFITM3 bands suggests that two (17.0 kDa) or four (34.0 kDa) molecules of ubiquitin are bound to embryonic IFITM3. All of these bands were eliminated when the blots were incubated in the absence of IFITM3 antibody (**Fig. 1A$_2$**, lanes 11, 12) and in the presence of pre-bound anti-IFITM3 (**Fig. 1A$_3$**, lanes 16, 17), with the exception of the robust band slightly above the 14.4 kDa standard band in the lane containing IFITM3-positive NIH 3T3 lysate treated with pre-bound primary antibody, which was nevertheless greatly diminished (**Fig. 1A$_3$**, lane 17). Incubated IFITM3 not pre-bound to the control peptide identified the same bands as the fresh primary antibody without any discernable decrease in signal (**Fig. 1A$_3$**, lanes 18, 19). Together, these data provide convincing evidence for specificity of anti-IFITM3.

IFITM3 antibody specificity was further verified in histological sections at 4-s (~E8.25), one of the stages during which IFITM3-positive cells were abundant in the allantois (**Fig. 1B**; see the following sections for details). Four reactions were carried out: (i) fresh primary anti-IFITM3 (**Fig. 1B**); (ii) elimination of the primary anti-IFITM3 (**Fig. 1C**), (iii) pre-binding the primary anti-IFITM3 with its cognate peptide sequence for 8 hours in the cold (**Fig. 1D**), and (iv) primary anti-IFITM3 alone, incubated for 8 hours in the cold (**Fig. 1E**). All regions that stained positively with the fresh IFITM3 antibody (**Fig. 1B**) were also positive in the incubated IFITM3 antibody (**Fig. 1D**) but were negative in both control reactions (**Fig. 1C, D**), indicating that IFITM3 signals are specific for all of the cell types and tissues described below.

Further antibody specificity was previously verified in *Ifitm3*-null tissue, as IFITM3 protein signal was absent in E12.5 mutant gonads but present in wildtype controls (Lange et al., 2008). While a product number for the Abcam anti-IFITM3 antibody listed in that study was not included in the Materials and Methods, M.A. Surani confirmed that it was ab15592 (personal communication), the same rabbit polyclonal antibody used in the current study.

2.2. IFITM3 protein exhibited distinct cellular localization profiles

IFITM3 has been reported to localize as a range of cellular profiles, including staining at the plasma membrane (Deblandre et al., 1995; Jia et al., 2012; Matsui and Okamura, 2005; Saitou et al., 2002), diffuse cytoplasmic staining (Bailey et al., 2012; Feeley et al., 2011; Yount et al., 2012; Yount et al., 2010), and concentrated cytoplasmic spots (Brass et al., 2009; Jia et al., 2012; Saitou et al., 2002; Yount et al., 2012). However, most of these data are from cultured cell lines. In the mouse conceptus, previous reports on the localization of IFITM3 protein have been limited to the putative PGC population, in which IFITM3 localized to the cell surface with a large cytoplasmic spot in the presumptive Golgi apparatus (Matsui and Okamura, 2005; Saitou et al., 2002). While *Ifitm3* expression has been documented in numerous other sites outside of the PGC trajectory (Lange et al., 2003; Tanaka and Matsui, 2002), the extent to which these other sites exhibit IFITM3 localization as cell surface staining with a large cytoplasmic spot, and/or as other cellular localization patterns, has not been considered.

Based on our systematic analysis of the mouse conceptus from ~E6.5-9.0, IFITM3 exhibited three types of cellular localization patterns, summarized broadly below. Localization to specific tissues will be described in subsequent sections 2.3-2.11.

Large cytoplasmic spots with cell surface staining—This cellular localization pattern (**Fig. 2A**), previously reported in the putative PGCs (Matsui and Okamura, 2005; Saitou et al., 2002), was not confined to the PGC trajectory; it was also found in other cells

of the posterior embryonic/extraembryonic junction, including *Flk1*-expressing endothelial cells and *Runx1*-expressing progenitor blood cells. Large cytoplasmic spots with cell surface staining were not detected outside of the posterior region.

Variable-sized cytoplasmic spots without cell surface staining—A large cytoplasmic spot (**Fig. 2B**) was found in a subset of tissues at stage-specific intervals, described below. In epithelial tissues, the large spot was localized to the cell's apical end (**Fig. 2C**), which is consistent with polarized localization of some proteins observed in epithelial cells (reviewed in Mellman and Nelson, 2008). A small cytoplasmic spot (**Fig. 2D**) localized to a subpopulation of cells in all tissues of the conceptus at all stages examined and will not be discussed further.

Widespread cellular staining—This staining, which included both the cytoplasm and the nucleus (**Fig. 3B**), was found in the visceral endoderm, both embryonic and extraembryonic, of the egg cylinder (Early-Late Streak, ES-LS, stages; ~E6.5-7.0), and was not consistent amongst specimens at the same morphological stages, with some conceptuses exhibiting widespread localization here, and others, hardly any at all. This category will not be discussed further in the Results section, but will be addressed in the Discussion (section 3).

2.3. PGC trajectory: proximal epiblast, Allantoic Core Domain (ACD)/intraembryonic primitive streak (IPS), and hindgut (~E6.5-9.0)

Upon initiation of the primitive streak (Early Streak, ES, stage; ~E6.5), IFITM3 localized as a large cytoplasmic spot within cells of the proximal epiblast (data not shown), consistent with previous reports of in situ hybridization for IFITM3 mRNA (Saitou et al., 2002). As the primitive streak elongated (Mid-Streak, MS, stage; ~E6.75), some IFITM3-positive cells persisted in the proximal epiblast (**Fig. 3A$_1$**) while others appeared to have moved posteriorly and were emerging from the primitive streak as nascent mesoderm (**Fig. 3A$_2$, B**). Extension of this cell population from the proximal epiblast to the primitive streak/mesoderm persisted through the Late Streak (LS) stage (~E7.0; data not shown).

As the posterior end of the primitive streak (extraembryonic primitive streak; XPS; Downs et al., 2009) extended into the newly-formed exocoelom (No Bud, OB, stage; ~E7.0), IFITM3-positive cells formed a cluster within it (**Fig. 3C**). All XPS IFITM3-positive cells contained a large cytoplasmic spot, but in some cells, the spot was accompanied by staining near the plasma membrane (**Fig. 3C**). By the allantoic bud stages (Early-Late Bud, EB-LB, stages; ~E7.25-7.5), the IFITM3-positive cluster in the XPS began to expand and extended into the embryonic region (**Fig. 3D**). An occasional cell in the elongating allantoic bud contained a large spot of IFITM3 (**Fig. 3D**). Throughout this period, posterior visceral endoderm (PVE) was negative for IFITM3 (**Fig. 3C, D**).

By the Early Headfold (EHF) stage (~E7.75), the posterior end of the primitive streak expands to create the Allantoic Core Domain (ACD), a stem/progenitor cell pool (Downs et al., 2009) that, together with the intraembryonic component of the posterior primitive streak (IPS), builds the posterior region of the conceptus (Mikedis and Downs, 2012). The ACD is subdivided into proximal and distal regions (Mikedis and Downs, 2012). The proximal region contributes to a variety of posterior fetal lineages and contains the majority of the allantois' STELLA-positive cells, and the distal region contributes primarily to the allantois (Mikedis and Downs, 2012). Posterior IFITM3 was observed as a large cytoplasmic spot, sometimes in conjunction with plasma membrane staining, in cells that extended from the distal ACD into the IPS (**Fig. 3E-G**). Here, in contrast to STELLA, which was found only in the proximal ACD, IFITM3-positive cells localized to both the proximal and distal regions

of the ACD (**Fig. 3E**). Intriguingly, while IFITM3-positive cells clustered within the ACD (**Fig. 3E, F_{1-2}**), those in the IPS were dispersed across the dorsal-ventral axis of the tissue (**Fig. 3E, F_3**). Whether the ACD's IFITM3-positive cells are actively displaced to the IPS, or whether they arise de novo in the IPS is not known. This IFITM3 staining pattern within the ACD and IPS persisted through the 5-s stage (~E8.25).

During this period, allantois- and IPS-associated PVE became positive for IFITM3 (**Fig. 3E, F**), exhibiting discrete IFITM3-postive cells containing large cytoplasmic spots with and without cell surface staining. This spatiotemporal localization pattern mirrors that of BRACHYURY (T; Downs et al., 2009), OCT-3/4 (Downs, 2008), and STELLA (Mikedis and Downs, 2012), all of which were also found in PVE by the headfold stage, but not before. In addition, from 1-4-s (~E8.0-8.25), occasional IFITM3-positive cells with a large cytoplasmic spot, and sometimes with plasma membrane staining, localized to the visceral endoderm of the yolk sac that is specifically associated with the ventral cuboidal mesothelium (VCM; data not shown), which forms the ventral proximal surface of the allantois (Daane et al., 2011). This small segment of visceral endoderm, which is just distal to the allantois-associated PVE, not only uniquely expresses Patched-1 (Daane and Downs, 2011), the major Hedgehog receptor (REF), but it also exhibits a squamous morphology similar to that of the PVE instead of the classical columnar morphology of yolk sac extraembryonic visceral endoderm (Daane et al., 2011).

By the 4-s stage (~E8.25), hindgut invagination begins; presumptive hindgut endoderm contained many IFITM3-positive cells, all of which exhibited the large cytoplasmic spot, and most of which included plasma membrane staining (**Fig. 3G**). By 6-8-s (~E8.5), the majority of IFITM3-positive cells were found in the ventral hindgut (**Fig. 3H**), but a few IFITM3-positive cells also localized in the dorsal hindgut, especially toward its caudal-most end (data not shown), similar to the localization pattern of STELLA (Mikedis and Downs, 2012). By 9-s (~E8.75), IFITM3 was confined to the ventral portion of the hindgut in the majority of specimens, where it primarily localized as a large cytoplasmic spot accompanied by plasma membrane staining; however, occasional cells were observed in the ventral hindgut with only a large cytoplasmic spot of IFITM3 (data not shown). IFITM3-positive cells in the hindgut remained confined to the ventral side through 14-s, when we terminated our study (**Fig. 3J**).

2.4. IFITM3 in the amnion and proximal epiblast (OB-5s; ~E7.0-8.25)

IFITM3 localized as a large cytoplasmic spot with occasional plasma membrane staining to the amniotic ectoderm (**Fig. 3C, D**) and dorsal epiblast (**Fig. 3D**) as early as the No Bud (OB) and Late Bud (LB) stages, respectively. Together, these formed a continuous population with IFITM3-positive cells of the XPS and IPS (**Fig. 3C, D**). In addition, some dorsal epiblast cells exhibited apically polarized staining (**Fig. 3D**). These localization patterns persisted in the amniotic ectoderm (**Fig. 3G**) and dorsal epiblast (**Fig. 3E**) through the 5-s stage. IFITM3 was never detected in amniotic mesoderm, where its cognate mRNA had been previously reported (Saitou et al., 2002). This discrepancy may be due to the ambiguities of whole mount analysis (Saitou et al., 2002), resolved here through examination of histological sections.

2.5. IFITM3 in the allantois at chorio-allantoic fusion (6-8s; ~E8.5) and beyond (9-14-s; ~E8.75-9.0)

By 6-8-s, concomitant with apparent loss/regression of the T-defined ACD (Downs et al., 2009) and completion of allantoic elongation, a population of IFITM3-positive cells persisted at the junction between the allantois and posterior embryo (**Fig. 3H**), all of which exhibited IFITM3 as a large cytoplasmic spot with or without plasma membrane staining. A

small number of cells with similar IFITM3 localization was also detected within the proximal allantoic midline, either as individual cells or as small clusters of a few cells (**Fig. 3H**), some of which were closely associated with the central allantoic arterial vessel (**Fig. 3G** and data not shown). From 9-14-s, when the allantois spreads over the chorionic surface and forms the highly branched vascular plexus of the placenta's labyrinth (reviewed in Inman and Downs, 2007), a few IFITM3-positive cells persisted in the allantois (**Fig. 3K**). In general, these IFITM3-positive cells appeared as single cells or as pairs of cells scattered throughout the allantois (**Fig. 3K**), from the posterior embryonic/extraembryonic junction to the portion of the allantois adjacent to the chorion. In addition, some cells localized to the flanks of the allantois (data not shown), while other cells were more centrally located within this tissue (**Fig. 3K**). All of these cells contained a cytoplasmic spot of IFITM3, accompanied in some by plasma membrane staining.

2.6. IFITM3 in the posterior embryo outside of the hindgut after chorio-allantoic fusion (9-14-s; ~E8.75-9.0)

Within the posterior embryo, the hindgut was not the exclusive site of IFITM3 localization; like STELLA (Mikedis and Downs, 2012), IFITM3 also localized to posterior sites in close proximity to the hindgut, specifically the posterior mesoderm (loose mesenchyme and somatopleure-associated mesoderm) (**Fig. 3J**), posterior surface ectoderm (**Fig. 3I**), and the VER (**Fig. 3J, K**), or remnant of the primitive streak that forms at ~E9.0 and is required for extending the tail posteriorly (Goldman et al., 2000; Grüneberg, 1956; Ohta et al., 2007; Tam and Tan, 1992; Wilson and Beddington, 1996). Within all of these tissues, IFITM3 localized as a large cytoplasmic spot with or without plasma membrane staining and, in the case of the posterior surface ectoderm and VER, as apical staining.

2.7. IFITM3 in anterior tissues

By the EHF stage, IFITM3 localized to the apical surface of some endodermal cells at the embryonic/extraembryonic junction of the anterior region (**Fig. 4A**). This small number of IFITM3-positive cells persisted there until 2-s (**Fig. 4B**), after which point, they began to expand in number to include endodermal cells overlying the developing heart (**Fig. 4C**). In addition, IFITM3 localized to the apical surface of some headfold neurectoderm at the EHF stage, and persisted there until 14-s (**Fig. 4A, B, D** and data not shown). Apical IFITM3 was also observed in the anterior embryo's surface ectoderm, which becomes apparent as early as 4-5-s onwards (**Fig. 4C**). Sporadic cells containing a large cytoplasmic spot of IFITM3 began to appear in head mesenchyme at the 3-5-s stage and persisted there through the 14-s stage (**Fig. 4D** and data not shown). At the Late Headfold (LHF) stage, anterior embryonic endoderm begins to invaginate to form the foregut. An occasional endodermal cell with IFITM3 on its apical surface was observed in the foregut region from LHF through 5-s (**Fig. 4C**).

Between 6-14-s, IFITM3 localized in a polarized manner within endoderm overlying the heart (**Fig. 4E**) as well as to a small population in the foregut opening (**Fig. 4E**) and in the ventral portion of the closed foregut (**Fig. 4F**). From 9-14-s, IFITM3 persisted in the surface ectoderm of the anterior embryo overlying neural crest tissue posterior to the nascent branchial arches (**Fig. 4G$_1$**). IFITM3 protein did not strongly localize to the branchial arches of the anterior embryo as only some of the mesodermal cells within the branchial arches contained a large cytoplasmic spot of IFITM3 (**Fig. 4G$_2$**). Intriguingly, as a previous study reported relatively strong *Ifitm3* expression in the branchial arches during this timeperiod (Lange et al., 2003; Tanaka and Matsui, 2002), mechanisms of translational repression (reviewed in Mendez and Richter, 2001; Villalba et al., 2011) may be acting on the *Ifitm3* mRNA in this tissue.

By 5-6-s, an occasional cell with a large cytoplasmic spot of IFITM3 was found in lateral mesoderm near the somites (**Fig. 4H** and data not shown). This occurred with increasing frequency at 7-8-s. By 9-s, IFITM3 was consistently observed as a cytoplasmic spot in lateral mesoderm adjacent to somites and persisted there through 14-s (**Fig. 4H** and data not shown).

2.8. IFITM3-positive cells contribute to Flk1-expressing cells

Intriguingly, from 9-14-s, IFITM3 localized to a small number of endothelial cells in the embryo proper (e.g., **Fig. 5A**), omphalomesenteric artery, blood islands of the yolk sac, and the umbilical veins (data not shown). Based on this localization pattern, and because we have found that STELLA-positive cells contribute to endothelial cells outside of the PGC trajectory (Mikedis and Downs, 2012), we hypothesized that IFITM3-positive cells would be found within vessel endothelium. Using the *Flk1*^{LacZ} reporter (3-6-s; N = 5) (Shalaby et al., 1995), IFITM3 co-localized with some *Flk1*-expressing cells in the allantois (**Fig. 5B$_1$**), anterior mesenchyme (**Fig. 5C**), and yolk sac hematopoietic cells (**Fig. 5D**) within the majority of specimens examined (**Table 1**). IFITM3 also colocalized with *Flk1* expression in the hindgut (**Fig. 5B$_2$**), which is consistent with previously reported expression of *Flk1* (Yamaguchi et al., 1993) and the major ligand of *Flk1, Vegf* (Miquerol et al., 1999), in definitive gut endoderm.

2.9. IFITM3 co-localizes with Runx1-expressing cells

IFITM3 localized as a large cytoplasmic spot to some hematopoietic cells of the yolk sac (**Fig. 5E**). This occasional staining was only observed in a subset of specimens at the initiation of yolk sac blood island formation (LB stage; ~E7.5), but by 10-14-s, each specimen had some yolk sac hematopoietic cells with a large cytoplasmic spot. Because of this localization, we hypothesized that IFITM3 might be co-expressed with *Runx1* in hematopoietic precursors in other regions of the conceptus, particularly within the allantois, which exhibits definitive hematopoietic potential (Zeigler et al., 2006) and whose ACD gives rise to hematopoietic cells that circulate within the posterior embryo (Mikedis and Downs, 2012). Using the *Runx1*^{LacZ} reporter (2-6-s; N = 6) (North et al., 1999; North et al., 2002), we observed co-localization of IFITM3 with *Runx1* expression in the allantois in all specimens examined (**Table 2; Fig. 5F**). Outside of the allantois, IFITM3 and *Runx1* co-localized in a majority of specimens within the IPS (**Fig. 5F**), posterior dorsal epiblast (**Fig. 5F**), amniotic ectoderm adjacent to posterior region, allantois- and IPS-associated PVE/hindgut (**Fig. 5F**), anterior endoderm overlying the heart, yolk sac hematopoietic cells (**Fig. 5G**), and VCM-associated yolk sac (**Table 2**).

We previously reported STELLA localization and *Runx1* expression within the VER (10-14-s; Daane and Downs, 2011; Mikedis and Downs, 2012), and thus, examined IFITM3 in the *Runx1*^{LacZ} reporter (8-13-s; N = 7). The majority of specimens exhibited IFITM3/*Runx1* co-localization in the VER (**Fig. 5I$_1$; Table 2**); this was accompanied by similar co-localization in the allantois (**Fig. 5I$_2$**), hindgut (**Fig. 5H**), endothelial cells, yolk sac hematopoietic cells, anterior endoderm overlying the heart, and foregut (**Table 2**). Within the hindgut, the IFITM3-positive, *Runx1*^{LacZ}-expressing cells localized to the ventral-most aspect of the hindgut (**Fig. 5H**), where they were found in close proximity to the *Runx1*-expressing omphalomesenteric artery (Daane and Downs, 2011).

2.10. IFITM3 in the extraembryonic visceral endoderm of the yolk sac

In a small number of cells within extraembryonic visceral endoderm in all specimens examined at all stages, IFITM3 localized to its vesicles as small, relatively lightly-stained spots (**Fig. 6A**) and as larger dark spots (**Fig. 3A$_2$, E**). In addition, an occasional IFITM3-

positive cell with a large cytoplasmic spot with or without plasma membrane staining localized to the extraembryonic visceral endoderm closely associated with the posterior region (data not shown) from 10-14-s.

2.11. IFITM3 in trophoblast giant cells

In contrast with other cell types, IFITM3 localization to the giant cells ranged from a dark cytoplasmic spot, to a dark cytoplasmic spot surrounded by lighter staining, to broad cytoplasmic staining (**Fig. 6B**). IFITM3 localization to the giant cells is consistent with giant cell production of interferon-α (Bany and Cross, 2006), which can upregulate *Ifitm3* expression (reviewed in Siegrist et al., 2011).

2.12. Subcellular localization of the IFITM3 spot

In human cell lines, cytoplasmic spots of IFITM3 were shown to be associated with the ER (Brass et al., 2009) and endolysosomes (Jia et al., 2012; Yount et al., 2012); in the posterior region of the mouse conceptus, they were claimed to be associated with the Golgi apparatus but no supporting evidence was presented (Saitou et al., 2002).

To elucidate the localization of cytoplasmic spots of IFITM3 within the cells of the mouse conceptus, IFITM3 was immunofluorescently colocalized at the 4-6-s stage (~E8.25-8.5) with ER marker calreticulin (CALR; **Fig. 7A, Table 3**), Golgi marker Golgi autoantigen (GOLGA1; **Fig. 7B, Table 3**), and endolysosomal marker lysosomal-associated membrane protein 1 (LAMP1; **Fig. 7C, Table 3**). IFITM3 spots were grouped based on their localization within the conceptus: posterior (which included spots with and without cell surface staining), lateral (only spots without cell surface staining), and anterior (primarily apical spots). Colocalization analysis via the Pearson correlation coefficient (PCC; see Methods) revealed that IFITM3 spots did not localize to the ER or endolysosomes within any region of the conceptus (PCC<0.5). Similarly, IFITM3 did not localize to the Golgi apparatus in the posterior or lateral regions of the conceptus (PCC<0.5). In the anterior embryo, the majority of spots did not localize to the Golgi apparatus (PCC<0.5), though 3 of 84 IFITM3 spots in the anterior embryo did exhibit colocalization with GOLGA1 (PCC>0.5 for these specimens; data not shown).

3. DISCUSSION

Previous studies examined IFITM3's involvement in PGC specification because *Ifitm3* mRNA was isolated from a subpopulation of posterior *Tnap*-expressing cells; not surprisingly, *Ifitm3*-expressing cells were subsequently found in the AP-defined putative PGC trajectory (Chiquoine, 1954) at the embryonic/allantoic junction, hindgut endoderm and gonads. Moreover, some *Ifitm3*-expressing cells found at the embryonic/extraembryonic junction also expressed *Stella*, whose expression (Lange et al., 2003; Saitou et al., 2002; Tanaka and Matsui, 2002) seemed to recapitulate that of AP. Those weakly *Ifitm3*-expressing cells which lacked *Stella* expression at the embryonic/extraembryonic junction were thought to contribute not to the germline but to somatic lineages (Saitou et al., 2002).

In light of our recent report that ACD- and IPS-derived STELLA-positive cells contribute to a range of posterior tissues, and were not limited to the putative PGC trajectory, we investigated IFITM3 localization by histological sections in the mouse gastrula at 2-4 hour developmental intervals over a 54-hour time period. Previous *Ifitm3* studies had been based on analysis of whole mount specimens, restricting signal detection to the most robust or clustered *Ifitm3* expression, such as the putative PGCs (**Fig. 3I**) and allantois (**Fig. 3C-G**), respectively. Consequently, *Ifitm3* expression might have been missed in potentially numerous other posterior tissues in which the mRNA localize more sporadically. As a result,

broader functions of IFITM3 in the gastrula were ignored. There is no question that systematic sectional analysis is superior to whole mount analysis in providing a more complete and unbiased mRNA or protein profile.

Results from the present study support the observation that posterior IFITM3 contributes to somatic lineages; however, while our study was not quantitative, relative levels of IFITM3 in posterior somatic tissues appeared just as high there as within the putative PGC trajectory. Thus, with the recent discovery of the Allantoic Core Domain, a stem/progenitor cell pool established by the posterior end of the primitive streak (Downs et al., 2009; Mikedis and Downs, 2012), we conclude that the phenotypic distinction between PGCs and posterior somatic cells remains obscure. Further work is needed to discover the extent to which IFITM3 distinguishes between putative PGCs and soma.

Intriguingly, broad cellular and nuclear IFITM3 staining was only detected in the yolk sac extraembryonic visceral endoderm and/or embryonic visceral endoderm in a subset of egg cylinder specimens (**Fig. 3B**). This difference in localization pattern may be due to the dissection medium's fetal calf serum, which contains interferon (Zamorska et al., 1977). Interferon can promote *Ifitm3* expression via the interferon-stimulable response elements that are upstream of the gene (Reid et al., 1989; Tanaka and Matsui, 2002). However, older specimens, including those stained within the same experiment as egg cylinder specimens, did not exhibit this variability, which suggests that, if the serum caused the upregulation of IFITM3 in the visceral endoderm of some egg cylinder specimens, these early gastrulae may be more sensitive to interferon than older ones. Another possibility is that egg cylinders may differentially respond to maternally-derived interferon found at implantation sites (Ashkar and Croy, 1999) or the interferon produced by the giant cells of the conceptus (Bany and Cross, 2006). Alternatively, as the interferon-stimulable response elements are dispensable for *Ifitm3* expression (Tanaka et al., 2004), it is also possible that *Ifitm3* is expressed in the streak-staged visceral endoderm by an interferon-independent mechanism. Finally, this apparently stochastic staining might reflect fluctuations in IFITM3 in the visceral endoderm over the 12 hour period represented by early to late streak-staged conceptuses. Indeed, we know from extensive experience that protein localization patterns within the posterior region are dynamic at intervals as short as 2 hours (e.g., Mikedis and Downs, 2009, 2012). Moreover, IFITM3 was absent from the PVE at the LB stage (~E7.5; **Fig. 3D**), but present there at the EHF stage (~E7.75; **Fig. 3E**).

The large cytoplasmic spot of IFITM3 (**Fig. 2A-C**) is reminiscent of the cellular staining pattern of another putative PGC marker, TNAP, which appears with or without cell surface staining in the putative PGC lineage (Ginsburg et al., 1990; Lawson and Hage, 1994; Mintz and Russell, 1957). While it has been claimed that this spot of TNAP distinguishes AP-positive putative PGCs from surrounding AP-positive soma (Ginsburg et al., 1990; Lawson and Hage, 1994; Mintz and Russell, 1957), there is no evidence for continuity between posterior TNAP-positive cells with or without the spot and the gonads in vivo. The spot of TNAP activity localizes to the Golgi apparatus (Clark and Eddy, 1975; Jeon and Kennedy, 1973), while TNAP activity at the plasma membrane staining originates from an accumulation of small electron-dense particles at the membrane (Clark and Eddy, 1975). Here, attempts to colocalize IFITM3 with proteins specific to the ER, Golgi and endolysosomes failed to clearly show IFITM3 within any one of these subcellular organelles. The nature of the spot is therefore unknown but perhaps IFITM3 overlaps “nuage”, a collection of perinuclear fibrillar material and dense core vesicles observed in putative hindgut PGCs by transmission electron microscopy (Clark and Eddy, 1975; Eddy, 1974, 1975; Spiegelman and Bennett, 1973). Whether nuage is characteristic of PGCs or even necessary for germ cell development in the mouse is obscure. However, nuage may not be sufficient for inducing the germline fate, as mispartitioned nuage (called P granules)

(reviewed in Voronina et al., 2011) in the *Caenorhabditis elegans* embryo does not make extra germ cells (Gallo et al., 2010). Moreover, in mice, loss of neither the entire IFITM family (Lange et al., 2008) nor TNAP (Macgregor et al., 1995) affects formation of the germ line or fertility.

Because IFITM3 is not required for germ line development, its role in the conceptus remains obscure. Beyond development, IFITM3 inhibits the replication of a range of viruses that enter the cell via endocytosis (Feeley et al., 2011; Huang et al., 2011; Weidner et al., 2010). While the placenta is an immunological organ that protects the fetus against infection (reviewed in Mor and Cardenas, 2010), transplacental passage and fetal infection in humans can occur on rare occasion with some viruses (reviewed in Bale, 2002). In such cases, the extent to which the fetus is able to fight infection remains obscure. Interferon is a key component of antiviral innate immunity (reviewed in Le Page et al., 2000), and the presence of IFITM3 in the early gastrula may serve as a poised state of innate immunity, ready to act in the event of viral infection, particularly within the critical populations to which IFITM3 localizes, including the putative PGCs (**Fig. 4I**), the putative stem cells of the ACD (**Fig. 4E**), some neural crest cells within the branchial arches (**Fig. 5G$_2$**), and the heart, via the IFITM3-positive overlying endoderm (**Fig. 5E**). The loss of this presumptive anti-viral protection may have contributed to the slight increase in morbidity among *Ifitm*-null mice compared to wildtype littermates observed exclusively at ~E17.5-perinatal stages, but not at earlier embryonic stages (Lange et al., 2008).

Western blot results presented here suggest that IFITM3 in the mouse conceptus may be post-translationally modified, but further work is needed to provide direct evidence. In HeLa cells transfected with an IFITM3 reporter plasmid, non-ubiquitinated and ubiquitinated IFITM3 is targeted to the endolysosomes and endoplasmic reticulum (ER) membrane, respectively, (Yount et al., 2012), while palmitoylated IFITM3 exhibits greater clustering within an organelle (Yount et al., 2010). Therefore, presumptive post-translational modifications may play a role in targeting IFITM3 to the plasma membrane or cytoplasmic spot in cells of the mouse conceptus.

Data from this study were collected from mice housed in a facility endemic for murine norovirus (MNV), which is widespread in research mouse facilities (Hsu et al., 2005) but is not pathogenic, except in immunodeficient mice (Karst et al., 2003; Ward et al., 2006). Though host resistance to MNV requires interferon-dependent pathways (Karst et al., 2003), this study's results were likely unaffected by MNV because intrauterine infection does not occur in non-immunodeficient, wildtype mice (Compton, 2008). In addition, though the infection status in previous *Ifitm3* expression studies was not indicated, our results generally accord with previous results (Lange et al., 2003; Saitou et al., 2002; Tanaka and Matsui, 2002).

In conclusion, though the profile of IFITM3 as a large cytoplasmic spot with plasma membrane staining was associated with the putative PGCs of the posterior primitive streak (the ACD and IPS) and hindgut, it was not unique to the PGC trajectory, as many somatic derivatives of the posterior primitive streak, specifically allantoic mesoderm, posterior mesoderm, posterior surface ectoderm, and VER (Mikedis and Downs, 2012), also exhibited this localization profile. The large cytoplasmic spot without plasma membrane staining was similarly identified along and surrounding the PGC trajectory and in some additional tissues of mesodermal and endodermal origin outside of the posterior region. This is consistent with the conclusion that, like STELLA (Mikedis and Downs, 2012), IFITM3 in the posterior region may identify a stem/progenitor cell population that contributes not only to the putative PGCs but also to multiple somatic lineages of the fetal-umbilical connection, and as

such, further obfuscates the distinction between PGCs and surrounding soma in the mouse gastrula.

4. EXPERIMENTAL PROCEDURES

4.1. Mouse strains, animal husbandry, dissection, and staging

All animals were treated in accordance with Public Health Service (PHS) Policy on Humane Care and Use of Laboratory Animals (Public Law 99-158) as enforced by the University of Wisconsin-Madison. Animals were maintained under a 12-hr light/dark cycle (lights out at 13:00 or 21:00) in an animal facility that is endemic for murine norovirus (MNV), but which is unlikely to infect non-immunodeficient wildtype embryos in utero (Compton, 2008). Estrus selection and mating were as previously summarized (Downs, 2006). Matings between the inbred hybrid strain B6CBAF1/J (The Jackson Laboratory, Bar Harbor, ME) provided the F_2 generation used in this study (Downs, 2006). Heterozygous *Kdr*^{tm1Jrt} (hereafter referred to as *Flk1*^{lacZ}) (Shalaby et al., 1995) and *Runx1*^{tm2Spe} (hereafter referred to as *Runx1*^{LacZ}) (North et al., 1999; North et al., 2002) males were mated with non-reporter B6CBAF1/J females to provide *Flk1*^{lacZ} (Inman and Downs, 2006) and *Runx1*^{LacZ} (Zeigler et al., 2006) specimens for further analysis as previously described. Pregnant females were sacrificed by cervical dislocation, conceptuses were dissected from decidua; parietal endoderm/Reichert's membrane and associated trophoblast were reflected; and embryos were staged (Downs and Davies, 1993) as follows: Early and Mid-Streak (ES, MS; ~E6.5-6.75); Late Streak and No (allantoic) Bud (LS, OB; ~E7.0); Early and Late (allantoic) Bud (EB, LB; ~E7.25-7.5); Early and Late Headfold (EHF, LHF; ~E7.75-8.0); 1-6-s (~E8.0-8.5); 7-8-s (~E8.5); 9-14-s (~E8.75-9.0).

4.2. Antibodies and blocking peptide

The following antibodies were used for Western blotting (WB), immunohistochemistry (IHC), and immunofluorescence (IF): Alexa Fluor 647-conjugated donkey anti-rabbit IgG secondary antibody (Jackson Immunoresearch Laboratories, Inc.; 711-605-152; 1.5 mg/mL stock; used at 1/250 dilution for IF); DyLight 550-conjugated donkey anti-goat IgG secondary antibody (Abcam; ab96932; 0.5 mg/mL stock; used at 1/250 dilution for IF); DyLight 550-conjugated donkey anti-sheep IgG secondary antibody (Abcam; ab96940; 0.5 mg/mL stock; used at 1/250 dilution for IF); anti-CALR (sheep polyclonal; Abcam; ab16144; 1.0 mg/mL; used at 1/50 for IF); anti-GOLGA1 (anti-GOLGIN 97; goat polyclonal; Santa Cruz Biotechnologies; sc-74632; 0.2 mg/mL; used at 1/50 for IF); anti-IFITM2/3 (rabbit polyclonal; Santa Cruz Biotechnologies; sc-66828; 0.2 mg/mL; used at 1/150 for WB); anti-IFITM3 (anti-FRAGILIS; rabbit polyclonal; Abcam; ab15592; 0.5 mg/mL stock; used at 1/500 for WB, 1/1250 for IHC, and 1/100 for IF); anti-LAMP1 (goat polyclonal; Santa Cruz Biotechnologies; sc-8098; 0.2 mg/mL; used at 1/5 for IF); biotinylated donkey anti-rabbit IgG secondary antibody (Santa Cruz Biotechnologies; sc-2089; 0.4 mg/mL stock; used at 1/500 for IHC); horseradish peroxidase-conjugated donkey anti-rabbit IgG secondary antibody (Santa Cruz Biotechnologies; sc-2313; 0.4 mg/ml stock; used at 1/5000 for WB). Blocking peptide controls for the IFITM3 primary antibody were conducted (Abcam; ab15737; 1.0 mg/mL stock; used at 1/100 for WB and 1/125 dilution for IHC).

For WB and IHC, control experiments verifying antibody specificity included elimination of primary antibody and pre-binding anti-IFITM3 with its cognate peptide (for WB, 1 hour at room temperature, N=1; for IHC, 8 hours at 4°C, N=3). Anti-IFITM3 simultaneously incubated without cognate protein for 1 hour at room temperature and 8 hours at 4°C exhibited signal as strong as the fresh IFITM3 antibody for WB and IHC analysis, respectively. For IF, control experiments included elimination of primary antibody (N=2).

4.3. Western blotting (WB)

Four litters of freshly dissected conceptuses (EHF-5-s; ~E7.75-8.25), divested of trophoblast giant cells, parietal endoderm, and the ectoplacental cone, were flash frozen, and total protein was extracted as previously described (Mysliwiec et al., 2007). Briefly, the conceptuses were homogenized and then subjected to sonication in buffer (0.2% SDS; 11% glycerol; 11mM Tris, pH 8.0; 1.1 mM EDTA, pH 8.0; 1 mM DTT; and a protease solution consisting of 0.02 mM leupeptin, 1.5 μM aprotinin, and 0.1 mM 4-(2-Aminoethyl) benzenesulfonyl fluoride hydrochloride (AEBSF). To detect IFITM3 protein, 10 μg of total protein extract was subjected to SDS-PAGE under reducing conditions in a 12% polyacrylamide gel, transferred to a polyvinylidene difluoride (PVDF) membrane (Immobilon-P Transfer Membrane; IPVH00010; EMD Millipore Corporation), and blocked in 10.0% milk/Tris-buffered saline (TBS)-Tween overnight at 4°C. The blot was then probed with IFITM3 primary antibody in 2.5% milk/TBS-Tween for 2 hours at room temperature, washed 3 times in TBS-Tween, probed with horseradish peroxidase-conjugated donkey anti-rabbit secondary antibody in 2.5% milk/TBS-Tween for 1 hour at room temperature, washed 3 times, and visualized via chemiluminescent detection (Amersham ECL Western blotting detection reagents; RPN2134; GE Healthcare) on Amersham Hyperfilm ECL (28906835; GE Healthcare). NIH 3T3 whole cell lysate (sc-2210; Santa Cruz Biotechnologies; 12.5 μg/lane) was used as a positive control (Bailey et al., 2012; Brass et al., 2009). To verify that the IFITM3 primary antibody did not detect IFITM2, WB was performed on 293T cell lysate transfected with mouse IFITM2 (sc-126995; Santa Cruz Biotechnologies; 7.5 μg/lane), for which nontransfected 293T cell lysate (sc-117752; Santa Cruz Biotechnologies; 7.5 μg/lane) served as a negative control. An anti-IFITM2/3 WB performed under the same conditions verified the presence of IFITM2 in the transfected 293T cell lysate. ECL Protein Molecular Weight Markers (RPN2280; GE Healthcare) were used according to manufacturer's instructions.

4.4. Immunohistochemistry (IHC)

To localize IFITM3, chromogenic IHC was carried out in whole mount specimens (•3 specimens/stage) as previously described (Downs, 2008), using anti-IFITM3 and biotinylated donkey anti-rabbit secondary antibody. Endogenous peroxidase activity was eliminated by incubating specimens in 5% hydrogen peroxide/methanol for 5 hours at room temperature (Downs, 2008). The antibody complex was visualized with diaminobenzoate chromagen (DAB; DAKO Corporation) at room temperature for 10 minutes, after which specimens were fixed in 4% paraformaldehyde (PFA) overnight at 4°C. Then, after standard dehydration and clearing, specimens were embedded in wax for transverse or sagittal orientations, sectioned at a thickness of 6 micrometers (microns, μm), dewaxed, lightly counterstained with hematoxylin, coverslipped, and analyzed.

4.5 Immunofluorescence (IF) and co-localization analysis

To verify the intracellular site(s) of IFITM3 localization, IF was carried out at 4-6-s stages (~E8.25-8.5; N=3 specimens). Whole mount specimens were blocked and incubated with primary and secondary antibodies as previously described (Downs, 2008), using primary antibodies against IFITM3 and markers for different organelles (CALR, GOLGA1, and LAMP1) with corresponding fluorophore-conjugated secondary antibodies. After the post-secondary antibody washes, specimens were counterstained with DNA marker DAPI (Life Technologies; D1306) at 1.8 μg/mL in phosphate-buffered saline (PBS) for 15 min at room temperature and then washed 3 times, 30 minutes each, in PBS. The posterior region containing the allantois, intraembryonic primitive streak (IPS), and overlying posterior visceral endoderm (PVE) was isolated using long glass scalpels (Tam and Beddington, 1992). The anterior embryo that contained the heart tube and foregut, as well as the lateral mesoderm posterior to the last somite, were similarly isolated. These tissue pieces were

individually mounted on glass slides in Aquamount (Lerner Laboratories; 13800) and gently coverslipped with no. 1.5 higher performance coverslips (170±5μm; Carl Zeiss Microscopy; 474030-9000).

Images were collected with a Plan Apo VC 60x water immersion objective (1.20 numerical aperature) using a 1.2 AU pinhole size set for the 638 nm (far red) laser on a Nikon A1R confocal microscope (W.M. Keck Laboratory for Biological Imaging, University of Wisconsin-Madison). Using the 408 nm, 561 nm, and 638 nm lasers, each image was collected twice, once via sequential scanning using the appropriate bandpass filters, and a second time via spectral detection settings, in which emission wavelengths 423-733 nm were collected at spectral bands of 10 nm via simultaneous exposure to all three lasers. Images from unlabeled and single fluorophore-labeled controls for each primary and secondary antibody combination, as well as for DAPI, were also collected using these settings. Images from sequential scanning were used to create panels for Fig. 7, but were not mathematically analyzed for colocalization. Spectral images were prepared and analyzed for colocalization using the NIS-Elements software version 4.00.03 (Nikon Instruments Inc.). Endogenous fluorescence from the tissue, as well as any residual crosstalk from the fluorophores' signals, was removed by performing spectral unmixing. Regions of interest (ROIs) from control spectral images were selected based on the presence of high fluorophore signal that was absent from non-labeled controls. Similarly, a background ROI was selected from a spectral image of the unlabeled control. The controls' ROIs were used to create a spectral library, which was then applied to spectrally unmix the triple fluorophore-labeled specimens.

On the unmixed images, a binary layer was created by thresholding the IFITM3 signal to 15.0% of its maximum intensity on the lower threshold and to the maximum level on the upper threshold. In addition, only signal regions of more than 1.0 μm^2 were included in the binary layer in order to exclude cell surface signal from the analysis. This binary layer was then used for colocalization analysis. Colocalization was mathematically analyzed via the Pearson correlation coefficient (PCC), which unlike an alternative colocalization measurement, Mander's overlap coefficient, does not identify colocalizing signals by favoring high intensities and downplaying combinations of low intensities or blank pixels (Adler and Parmryd, 2010). Furthermore, because pixels were only analyzed for colocalization if they contained IFITM3 signal that was part of a cytoplasmic spot, blank pixels were excluded from the analysis, thereby circumventing a limitation of the PCC, its sensitivity to blank pixels (Adler and Parmryd, 2010).

Acknowledgments

The authors thank Lance Rodenkirch (W.M. Keck Laboratory for Biological Imaging, University of Wisconsin-Madison) and Colleen Lavin (Nikon Instruments Inc.) for expert assistance with the colocalization study. This study was supported by a grant from the National Institutes of Child Health and Development (R01 HD042706) to K.M.D. M.M.M. is a National Science Foundation Graduate Research Fellow and was further supported by a pre-doctoral fellowship from the Stem Cell and Regenerative Medicine Center at the University of Wisconsin-Madison School of Medicine and Public Health.

ABBREVIATIONS

ACD	Allantoic Core Domain
AP	alkaline phosphatase
CALR	careticulin
EB	Early (allantoic) Bud
ES	Early Streak

EHF	Early Headfold
ER	endoplasmic reticulum
Flk1	fetal liver kinase 1
GOLGA1	Golgi autoantigen
IF	immunofluorescence
IHC	immunohistochemistry
IFITM2	interferon-induced transmembrane protein 2
IFITM3	interferon-induced transmembrane protein 3
IPS	intraembryonic posterior primitive streak
LAMP1	lysosomal-associated membrane protein 1
LB	Late (allantoic) Bud
LHF	Late Headfold
LS	Late Streak
MS	Mid-Streak
OB	No (allantoic) Bud
PCC	Pearson correlation coefficient
PGCs	primordial germ cells
PRDM1	PR domain zinc finger protein 1
PVE	posterior visceral endoderm
Runx-1	Runt-related transcription factor 1
s	somite pairs
TNAP	tissue-nonspecific alkaline phosphatase
VCM	ventral cuboidal mesothelium
VER	ventral ectodermal ridge
XPS	extraembryonic posterior primitive streak

REFERENCES

Adler J, Parmryd I. Quantifying Colocalization by Correlation: The Pearson Correlation Coefficient is Superior to the Mander's Overlap Coefficient. Cytometry Part A. 2010; 77A:733–742.

Ashkar AA, Croy BA. Interferon-gamma contributes to the normalcy of murine pregnancy. Biology of Reproduction. 1999; 61:493–502. [PubMed: 10411532]

Bailey CC, Huang IC, Kam C, Farzan M. Ifitm3 limits the severity of acute influenza in mice. PLoS Pathog. 2012; 8:e1002909–e1002909. [PubMed: 22969429]

Bale JF. Congenital infections. Neurol. Clin. 2002; 20:1039–+. [PubMed: 12616680]

Bany BM, Cross JC. Post-implantation mouse conceptuses produce paracrine signals that regulate the uterine endometrium undergoing decidualization. Developmental Biology. 2006; 294:445–456. [PubMed: 16616120]

Beddington RSP. Induction of a second neural axis by the mouse node. Development. 1994; 120:613–620. [PubMed: 8162859]

Benham FJ, Wiles MV, Goodfellow PN. Differentiation in vitro of human-mouse teratocarcinoma hybrids. Mol. Cell. Biol. 1983; 3:2259–2270. [PubMed: 6686281]

Bernstine EG, Hooper ML, Grandchamp S, Ephrussi B. Alkaline phosphatase activity in mouse teratoma. Proceedings of the National Academy of Sciences of the United States of America. 1973; 70:3899–3903. [PubMed: 4521215]

Bortvin A, Goodheart M, Liao M, Page DC. Dppa3 / Pgc7 / stella is a maternal factor and is not required for germ cell specification in mice. BMC Developmental Biology. 2004; 4:2. [PubMed: 15018652]

Bowles J, Teasdale RP, James K, Koopman P. Dppa3 is a marker of pluripotency and has a human homologue that is expressed in germ cell tumours. Cytogenet. Genome Res. 2003; 101:261–265. [PubMed: 14684992]

Brass AL, Huang IC, Benita Y, John SP, Krishnan MN, Feeley EM, Ryan BJ, Weyer JL, van der Weyden L, Fikrig E, Adams DJ, Xavier RJ, Farzan M, Elledge SJ. The IFITM Proteins Mediate Cellular Resistance to Influenza A H1N1 Virus, West Nile Virus, and Dengue Virus. Cell. 2009; 139:1243–1254. [PubMed: 20064371]

Carter MG, Stagg CA, Falco G, Yoshikawa T, Bassey UC, Aiba K, Sharova LV, Shaik N, Ko MSH. An in situ hybridzation-based screen for heterogeneously expressed genes in mouse ES cells. Gene Expression Patterns. 2008; 8:181–198. [PubMed: 18178135]

Chiquoine AD. The identification, origin, and migration of the primordial germ cells in the mouse embryo. Anat. Rec. 1954; 118:135–146. [PubMed: 13138919]

Clark JM, Eddy EM. Fine structural observations on the origin and associations of primordial germ cells of the mouse. Developmental Biology. 1975; 47:136–155. [PubMed: 173592]

Compton SR. Prevention of murine norovirus infection in neonatal mice by fostering. J. Amer. Assoc. Lab. Anim. Sci. 2008; 47:25–30. [PubMed: 18459709]

Daane JM, Downs KM. Hedgehog signaling in the posterior region of the mouse gastrula suggests manifold roles in the fetal-umbilical connection and posterior morphogenesis. Developmental Dynamics. 2011; 240:2175–2193. [PubMed: 22016185]

Daane JM, Enders AC, Downs KM. Mesothelium of the murine allantois exhibits distinct regional properties. Journal of Morphology. 2011; 272:536–556. [PubMed: 21284019]

Deblandre GA, Marinx OP, Evans SS, Majjaj S, Leo O, Caput D, Huez GA, Wathelet MG. Expression cloning of an interferon-inducible 17-kDa membrane protein implicated in the control of cell growth. Journal of Biological Chemistry. 1995; 270:23860–23866. [PubMed: 7559564]

Downs KM. Systematic localization of Oct-3/4 to the gastrulating mouse conceptus suggests manifold roles in mammalian development. Developmental Dynamics. 2008; 237:464–475. [PubMed: 18213575]

Downs KM, Davies T. Staging of gastrulating mouse embryos by morphological landmarks in the dissecting microscope. Development. 1993; 118:1255–1266. [PubMed: 8269852]

Downs KM, Inman KE, Jin DX, Enders AC. The Allantoic Core Domain: New insights into the development of the murine allantois and its relation to the primitive streak. Developmental Dynamics. 2009; 238:532–553. [PubMed: 19191225]

Eddy EM. Fine structural observations on form and distribution of nuage in germ cells of rat. Anat. Rec. 1974; 178:731–757. [PubMed: 4815140]

Eddy EM. Germ plasm and differentiation of germ cell line. Int.Rev.Cytol. 1975; 43:229–280. [PubMed: 770367]

Feeley EM, Sims JS, John SP, Chin CR, Pertel T, Chen LM, Gaiha GD, Ryan BJ, Donis RO, Elledge SJ, Brass AL. IFITM3 Inhibits Influenza A Virus Infection by Preventing Cytosolic Entry. PLoS Pathog. 2011; 7

Gallo CM, Wang JT, Motegi F, Seydoux G. Cytoplasmic Partitioning of P Granule Components Is Not Required to Specify the Germline in C. elegans. Science. 2010; 330:1685–1689. [PubMed: 21127218]

Ginsburg M, Snow MHL, McLaren A. Primordial germ cells in the mouse embryo during gastrulation. Development. 1990; 110:521–528. [PubMed: 2133553]

Goldman DC, Martin GR, Tam PPL. Fate and function of the ventral ectodermal ridge during mouse tail development. Development. 2000; 127:2113–2123. [PubMed: 10769235]

Grüneberg H. A ventral ectodermal ridge of the tail in mouse embryos. Nature. 1956; 177:787–788. [PubMed: 13321960]

Hasselgren PO, Fischer JE. The ubiquitin-proteasome pathway - Review of a novel intracellular mechanism of muscle protein breakdown during sepsis and other catabolic conditions. Ann. Surg. 1997; 225:307–316. [PubMed: 9060588]

Hayashi K, Lopes S, Surani MA. Germ cell specification in mice. Science. 2007; 316:394–396. [PubMed: 17446386]

Horsley V, O'Carroll D, Tooze R, Ohinata Y, Saitou M, Obukhanych T, Nussenzweig M, Tarakhovsky A, Fuchs E. Blimp1 defines a progenitor population that governs cellular input to the sebaceous gland. Cell. 2006; 126:597–609. [PubMed: 16901790]

Hsu CC, Wobus CE, Steffen EK, Riley LK, Livingston RS. Development of a microsphere-based serologic multiplexed fluorescent immunoassay and a reverse transcriptase PCR assay to detect murine norovirus 1 infection in mice. Clin. Diagn. Lab. Immunol. 2005; 12:1145–1151. [PubMed: 16210475]

Huang IC, Bailey CC, Weyer JL, Radoshitzky SR, Becker MM, Chiang JJ, Brass AL, Ahmed AA, Chi XL, Dong LA, Longobardi LE, Boltz D, Kuhn JH, Elledge SJ, Bavari S, Denison MR, Choe H, Farzan M. Distinct Patterns of IFITM-Mediated Restriction of Filoviruses, SARS Coronavirus, and Influenza A Virus. PLoS Pathog. 2011; 7

Inman KE, Downs KM. Brachyury is required for elongation and vasculogenesis in the murine allantois. Development. 2006; 133:2947–2959. [PubMed: 16835439]

Inman KE, Downs KM. The murine allantois: Emerging paradigms in development of the mammalian umbilical cord and its relation to the fetus. Genesis. 2007; 45:237–258. [PubMed: 17440924]

Jaiswal N, Haynesworth SE, Caplan AI, Bruder SP. Osteogenic differentiation of purified, culture-expanded human mesenchymal stem cells in vitro. J. Cell. Biochem. 1997; 64:295–312. [PubMed: 9027589]

Jeon KW, Kennedy JR. The primoridal germ cells in early mouse embryos: light and electron microscopic studies. Developmental Biology. 1973; 31:275–284. [PubMed: 4787198]

Jia R, Pan Q, Ding S, Rong L, Liu S-L, Geng Y, Qiao W, Liang C. The N-Terminal Region of IFITM3 Modulates Its Antiviral Activity by Regulating IFITM3 Cellular Localization. Journal of Virology. 2012; 86:13697–13707. [PubMed: 23055554]

Karst SM, Wobus CE, Lay M, Davidson J, Virgin HW. STAT1-dependent innate immunity to a Norwalk-like virus. Science. 2003; 299:1575–1578. [PubMed: 12624267]

Lange UC, Adams DJ, Lee C, Barton S, Schneider R, Bradley A, Surani MA. Normal germ line establishment in mice carrying a deletion of the Ifitm/Fragilis gene family cluster. Mol. Cell. Biol. 2008; 28:4688–4696. [PubMed: 18505827]

Lange UC, Saitou M, Western PS, Barton SC, Surani MA. The Fragilis interferon-inducible gene family of transmembrane proteins is associated with germ cell specification in mice. BMC Developmental Biology. Mar 19.2003 3 2003.

Lawson, KA.; Hage, WJ. Clonal analysis of the origin of primordial germ cells in the mouse. In: Chadwick, DJ.; Marsh, J., editors. Germline Development. Wiley; Chichester: 1994. p. 68-84.

Le Page C, Genin P, Baines MG, Hiscott J. Interferon activation and innate immunity. Reviews in immunogenetics. 2000; 2:374–386. [PubMed: 11256746]

Lewinson D, Toister Z, Silbermann M. Quantitative and distributional changes in the activity of alkaline phosphatase during the maturation of cartilage. J. Histochem. Cytochem. 1982; 30:261–269. [PubMed: 7061826]

Macgregor GR, Zambrowicz BP, Soriano P. Tissue nonspecific alkaline phosphatase is expressed in both embryonic and extraembryonic lineages during mouse embryogenesis but is not required for migration of primordial germ cells. Development. 1995; 121:1487–1496. [PubMed: 7789278]

Matsui Y, Okamura D. Mechanisms of germ-cell specification in mouse embryos. Bioessays. 2005; 27:136–143. [PubMed: 15666347]

McLaren A. Establishment of the germ cell lineage in mammals. J. Cell. Physiol. 2000; 182:141–143. [PubMed: 10623876]

Mellman I, Nelson WJ. Coordinated protein sorting, targeting and distribution in polarized cells. Nat. Rev. Mol. Cell Biol. 2008; 9:833–845. [PubMed: 18946473]

Mendez R, Richter JD. Translational control by CPEB: A means to the end. Nat. Rev. Mol. Cell Biol. 2001; 2:521–529. [PubMed: 11433366]

Mikedis MM, Downs KM. Collagen type IV and Perlecan exhibit dynamic localization in the Allantoic Core Domain, a putative stem cell niche in the murine allantois. Developmental Dynamics. 2009; 238:3193–3204. [PubMed: 19924818]

Mikedis MM, Downs KM. STELLA-positive subregions of the primitive streak contribute to posterior tissues of the mouse gastrula. Developmental Biology. 2012; 363:201–218. [PubMed: 22019303]

Mintz B, Russell ES. Gene-induced embryological modifications of primordial germ cells in the mouse. Journal of Experimental Zoology. 1957; 134:207–237. [PubMed: 13428952]

Miquerol L, Gertsenstein M, Harpal K, Rossant J, Nagy A. Multiple developmental roles of VEGF suggested by a LacZ-tagged allele. Developmental Biology. 1999; 212:307–322. [PubMed: 10433823]

Mor G, Cardenas I. The Immune System in Pregnancy: A Unique Complexity. American Journal of Reproductive Immunology. 2010; 63:425–433. [PubMed: 20367629]

Mould A, Morgan MAJ, Li L, Bikoff EK, Robertson EJ. Blimp1/Prdm1 governs terminal differentiation of endovascular trophoblast giant cells and defines multipotent progenitors in the developing placenta. Genes & Development. 2012; 26:2063–2074. [PubMed: 22987638]

Mysliwiec MR, Kim T, Lee Y. Characterization of zinc finger protein 496 that interacts with Jumonji/Jarid2. FEBS Lett. 2007; 581:2633–2640. [PubMed: 17521633]

Nishikawa K, Nakashima T, Hayashi M, Fukunaga T, Kato S, Kodama T, Takahashi S, Calame K, Takayanagi H. Blimp1-mediated repression of negative regulators is required for osteoclast differentiation. Proceedings of the National Academy of Sciences of the United States of America. 2010; 107:3117–3122. [PubMed: 20133620]

North T, Gu TL, Stacy T, Wang Q, Howard L, Binder M, Marin-Padilla M, Speck NA. Cbfa2 is required for the formation of intra-aortic hematopoietic clusters. Development. 1999; 126:2563–2575. [PubMed: 10226014]

North TE, de Bruijin M, Stacy T, Talebian L, Lind E, Robin C, Binder M, Dzierzak E, Speck NA. Runx1 expression marks long-term repopulating hematopoietic stem cells in the midgestation mouse embryo. Immunity. 2002; 16:661–672. [PubMed: 12049718]

Ohinata Y, Payer B, O'Carroll D, Ancelin K, Ono Y, Sano M, Barton SC, Obukhanych T, Nussenzweig M, Tarakhovsky A, Saitou M, Surani MA. Blimp1 is a critical determinant of the germ cell lineage in mice. Nature. 2005; 436:207–213. [PubMed: 15937476]

Ohta S, Suzuki K, Tachibana K, Tanaka H, Yamada G. Cessation of gastrulation is mediated by suppression of epithelial-mesenchymal transition at the ventral ectodermal ridge. Development. 2007; 134:4315–4324. [PubMed: 18003744]

Payer B, Saitou M, Barton SC, Thresher R, Dixon JPC, Zahn D, Colledge WH, Carlton MBL, Nakano T, Surani MA. stella is a maternal effect gene required for normal early development in mice. Curr. Biol. 2003; 13:2110–2117. [PubMed: 14654002]

Reid LE, Brasnett AH, Gilbert CS, Porter ACG, Gewert DR, Stark GR, Kerr IM. A single DNA response element can confer inducibility by both alpha- and gamma-interferons. Proceedings of the National Academy of Sciences of the United States of America. 1989; 86:840–844. [PubMed: 2492664]

Saitou M, Barton SC, Surani MA. A molecular programme for the specification of germ cell fate in mice. Nature. 2002; 418:293–300. [PubMed: 12124616]

Shalaby F, Rossant J, Yamaguchi TP, Gertsenstein M, Wu XF, Breitman ML, Schuh AC. Failure of blood island formation and vasculogenesis in Flk-1-deficient mice. Nature. 1995; 376:62–66. [PubMed: 7596435]

Siegrist F, Ebeling M, Certa U. The Small Interferon-Induced Transmembrane Genes and Proteins. Journal of Interferon and Cytokine Research. 2011; 31:183–197. [PubMed: 21166591]

Spiegelman M, Bennett D. A light- and electron-microscopic study of primordial germ cells in the early mouse embryo. Journal of Embryology and Experimental Morphology. 1973; 30:97–118. [PubMed: 4729955]

Tam PPL, Beddington RSP. Establishment and organization of germ layers in the gastrulating mouse embryo. Postimplantation Development in the Mouse. 1992; 165:27–49.

Tam PPL, Tan SS. The somitogenetic potential of cells in the primitive streak and the tail bud of the organogenesis-stage mouse embryo. Development. 1992; 115:703–715. [PubMed: 1425350]

Tanaka SS, Matsui Y. Developmentally regulated expression of mil-1 and mil-2, mouse interferon-induced transmembrane protein like genes, during formation and differentiation of primordial germ cells. Mechanisms of Development. 2002; 119:S261–S267. [PubMed: 14516695]

Tanaka SS, Nagamatsu G, Tokitake Y, Kasa M, Tam PPL, Matsui Y. Regulation of expression of mouse interferon induced transmembrane protein like gene-3, Ifitm3 (mil-1, fragilis), in germ cells. Developmental Dynamics. 2004; 230:651–659. [PubMed: 15254899]

Turner CA, Mack DH, Davis MM. Blimp-1, a novel zinc finger-containing protein that can drive the maturation of B lymphocytes into immunoglobulin-secreting cells. Cell. 1994; 77:297–306. [PubMed: 8168136]

Villalba A, Coll O, Gebauer F. Cytoplasmic polyadenylation and translational control. Curr. Opin. Genet. Dev. 2011; 21:452–457. [PubMed: 21536428]

Vincent SD, Dunn NR, Sciammas R, Shapiro-Shalef M, Davis MM, Calame K, Bikoff EK, Robertson EJ. The zinc finger transcriptional repressor Blimp1/Prdm1 is dispensable for early axis formation but is required for specification of primordial germ cells in the mouse. Development. 2005; 132:1315–1325. [PubMed: 15750184]

Voronina E, Seydoux G, Sassone-Corsi P, Nagamori I. RNA Granules in Germ Cells. Cold Spring Harbor Perspectives in Biology. 2011; 3

Ward JM, Wobus CE, Thackray LB, Erexson CR, Faucette LJ, Belliot G, Barron EL, Sosnovtsev SV, Green KY. Pathology of immunodeficient mice with naturally occurring murine norovirus infection. Toxicol. Pathol. 2006; 34:708–715. [PubMed: 17074739]

Weidner JM, Jiang D, Pan XB, Chang JH, Block TM, Guo JT. Interferon-Induced Cell Membrane Proteins, IFITM3 and Tetherin, Inhibit Vesicular Stomatitis Virus Infection via Distinct Mechanisms. Journal of Virology. 2010; 84:12646–12657. [PubMed: 20943977]

Wilson V, Beddington RSP. Cell fate and morphogenetic movement in the late mouse primitive streak. Mechanisms of Development. 1996; 55:79–89. [PubMed: 8734501]

Yamaguchi TP, Dumont DJ, Conlon RA, Breitman ML, Rossant J. Flk-1, an Flt-related receptor tyrosine kinase is an early marker for endothelial cell precursors. Development. 1993; 118:489–498. [PubMed: 8223275]

Yount JS, Karssemeijer RA, Hang HC. S-Palmitoylation and Ubiquitination Differentially Regulate Interferon-induced Transmembrane Protein 3 (IFITM3)-mediated Resistance to Influenza Virus. The Journal of biological chemistry. 2012; 287:19631–19641. [PubMed: 22511783]

Yount JS, Moltedo B, Yang YY, Charron G, Moran TM, Lopez CB, Hang HC. Palmitoylome profiling reveals S-palmitoylation-dependent antiviral activity of IFITM3. Nat. Chem. Biol. 2010; 6:610–614. [PubMed: 20601941]

Zamorska B, Kolaczkowska MK, Biernacka I, Lobodzinska M. Rat interferons - Homologous and heterologus rat serum activity. Arch. Immunol. Ther. Exp. 1977; 25:515–520.

Zeigler BM, Sugiyama D, Chen M, Guo YL, Downs KM, Speck NA. The allantois and chorion, when isolated before circulation or chorio-allantoic fusion, have hematopoietic potential. Development. 2006; 133:4183–4192. [PubMed: 17038514]

HIGHLIGHTS

1. IFITM3 was immuno-localized to histological sections of the mouse gastrula.
2. IFITM3 exhibited regionally-specific cellular localization profiles.
3. Of these profiles, none was confined to the putative PGC trajectory.
4. Cells with relatively high IFITM3 localized to posterior streak-derived tissues.
5. Other cellular profiles of relatively less IFITM3 were not regionally specific.

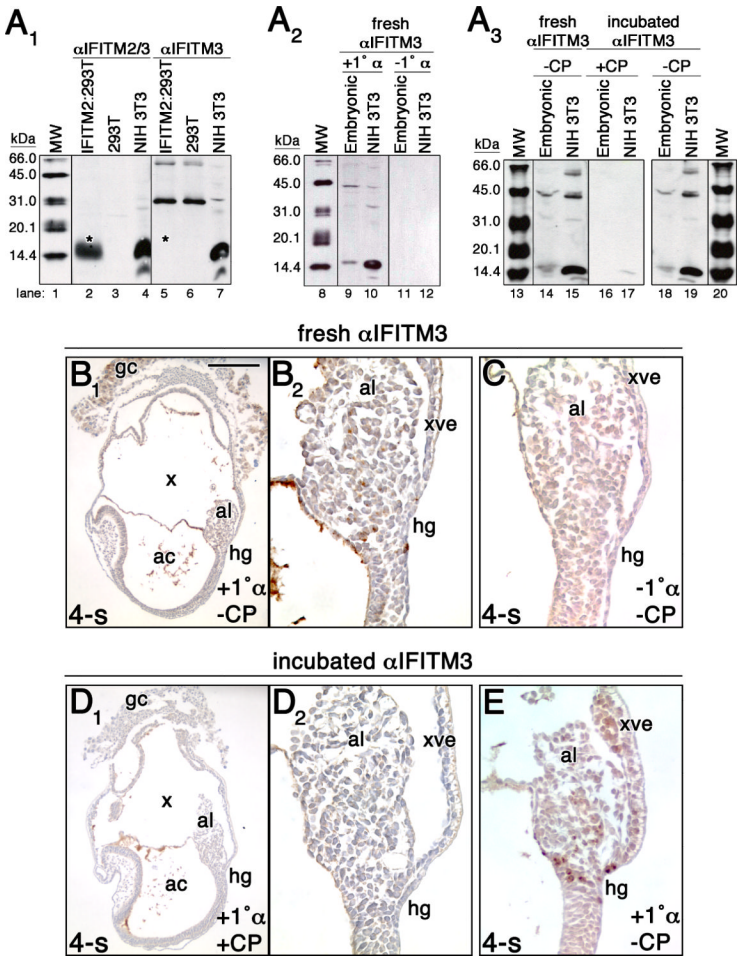

Fig. 1. Specificity of IFITM3 antibody

A: IFITM3 Western blots. Each panel represents a single exposure collected from a single blot, with line divisions indicating lanes whose order within the blot has been digitally shifted for clarity. Molecular weight (MW) relationships among lanes within each blot have been maintained. For each blot, lanes 1, 8, 13, and 20: MW ladder (please see Methods); NIH 3T3 cell lysate served as a positive control for the presence of IFITM3 (please see Results/Methods). **A_1:** Anti (α)-IFITM2/3 verified the presence of mouse IFITM2 near its predicted MW of 15.7 kDa in transfected 293T cell lysate (**A_1**, lane 2, below asterisk), its absence in non-transfected 293T cell lysate (**A_1**, lane 3), and its presence in NIH 3T3 lysate (**A_1**, lane 4). Anti-IFITM3 did not identify IFITM2 at this MW in the transfected IFITM2:293T cells (**A_1**, lane 5, below asterisk), but did identify bands at ~31 and ~66 kDa (**A_1**, lane 5); however, these bands were also present in the non-transfected 293T extract (**A_1**, lane 6), which does not contain IFITM2. **A_2:** Total protein extracts from mouse gastrulae (see Experimental Procedures; EHF-6-s; ~E7.75-8.5; **A_2**, lane 9) and from NIH 3T3 cells (**A_2**, lane 10) probed with anti-IFITM3 each contain a band just above the 14.4 kDa ladder mark, consistent with a predicted MW of 15.0 kDa for IFITM3. The total embryonic lysate contains one additional band of higher molecular weight (**A_2**, lane 9), while NIH 3T3 lysate contains three additional bands of higher molecular weight (**A_2**, lane 10). NIH 3T3 lysate also contained an additional band below the 14.4 kDa ladder mark that may represent a degradation product of IFITM3. Probing the same amount of protein extract in the absence of anti-IFITM3 (-1° α) eliminated all of the bands (**A_2**, lanes 11-12). **A_3:** Total protein extracts from mouse gastrulae (see Materials and Methods; EHF-5-s;

~E7.75-8.25; **A_3**, lane 14) and from NIH 3T3 cells (**A_3**, lane 15) probed with anti-IFITM3 (-CP: anti-IFITM3 not pre-bound to control peptide) each contain a band slightly above the 14.4 kDa ladder mark that is consistent with a predicted MW of 15.0 kDa for IFITM3. The total embryonic lysate contains one additional bands of higher molecular weight (**A_3**, lane 14), while NIH 3T3 cell lysate contains three additional bands of higher molecular weight and one band of lower molecular weight (**A_3**, lane 15). Probing the same amount of protein extract with anti-IFITM3 pre-bound to the control peptide (+CP; **A_3**, lanes 16-17) eliminated all of the bands, except for the NIH 3T3 band slightly above the 14.4 kDa ladder mark, though this band was significantly diminished in intensity (**A_3**, lane 17). Incubated anti-IFITM3 not pre-bound to the control peptide (**Fig. 1A_3**, lanes 18, 19) identified the same bands as the fresh anti-IFITM3 (**Fig. 1A_3**, lanes 14, 15), demonstrating that the incubation did not reduce the reactivity of anti-IFITM3. Differences in the intensities of bands in the NIH 3T3 lanes in panels $A_{1\text{-}3}$ may reflect the different lots of NIH 3T3 protein used in these experiments. **B-E:** 4-s stage (~8.25). Unless otherwise indicated, all sections presented here and in subsequent figures are sagittal with anterior on the left and posterior on the right. IFITM3 immunostaining is brown, and all sections were counterstained in hematoxylin (blue color). **B:** Staining with fresh anti-IFITM3 not pre-bound to control peptide (-CP) at low (**B_1**) and high (**B_2**) magnification. **C:** Staining in the absence of anti-IFITM3 (-1° α). **D:** Staining with incubated anti-IFITM3 pre-bound to control peptide (+CP) at low (**C_1**) and high (**C_2**) magnification. **E:** Staining with incubated anti-IFITM3 not pre-bound to the control peptide (-CP). Other abbreviations: ac, amniotic cavity; al, allantois; gc, giant cells; hg, hindgut invagination; x, exocoelom; xve, extraembryonic visceral endoderm. Scale bar in B_1: 200 μm (B_1, D_1); 50 μm (B_2, C, D_2, E).

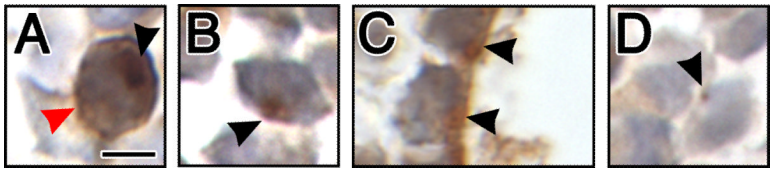

Fig. 2. Localization profiles of IFITM3 protein

A: Cytoplasmic spot (black arrowhead) with staining in the plasma membrane (red arrowhead). Cell enlarged from the intraembryonic primitive streak (IPS) of 5-s-staged specimen in Fig. 3B. **B:** Large cytoplasmic spot (black arrowhead). Cell enlarged from the proximal allantois of 4-s-staged specimen in Fig. $1B_2$. **C:** Apical localization (black arrowheads). Cell enlarged from posterior surface ectoderm of 10-s-staged specimen in Fig. 3I. **D:** Small cytoplasmic spot (black arrowhead). Cell enlarged from the IPS of 4-s staged specimen in Fig. $1B_2$. Scale bar in A: 5.0 μm (A-D).

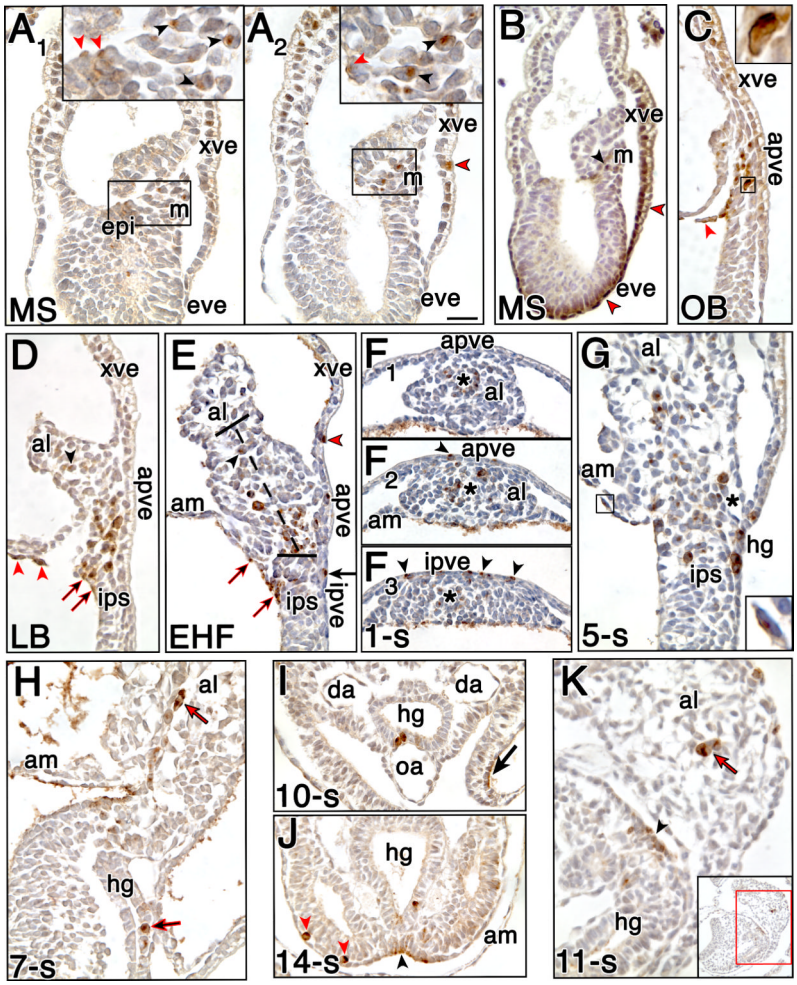

Fig. 3. IFITM3 along the trajectory of the putative PGCs, as well as in the allantois and other posterior tissues (Mid-streak (MS)-14-s; ~E6.75-9.0)

A: MS stage; A_1 and A_2 are two different sections from the same specimen; A_1 shows more epiblast-positive IFITM3, while A_2 shows more positive mesoderm. IFITM3 localized as a cytoplasmic spot to the proximal epiblast (epi; insets, red arrowheads) as well as to the primitive streak and posterior mesoderm (m; insets, black arrowheads). IFITM3 also localized to some vesicles of extraembryonic visceral endoderm (xve; red arrowheads outlined in black; A_2), which was the extent of the staining observed in the visceral endoderm of this specimen. Black boxes designate regions magnified within insets. **B:** MS stage. IFITM3 localized as a cytoplasmic spot to posterior mesoderm (black arrowhead). In addition, IFITM3 exhibited broad nuclear and cytoplasmic staining in the visceral endoderm (red arrowheads outlined in black), both embryonic (eve) and extraembryonic (xve), that was observed in only a subset of egg cylinder specimens, but not in older specimens. **C:** No Bud/Neural Plate (OB) stage (~E7.0). IFITM3 primarily localized as cytoplasmic spots with (inset) or without plasma membrane staining to the extraembryonic extension of the primitive streak (XPS), the triangular wedge of tissue above the amnion and adjacent to the allantois-associated posterior visceral endoderm (apve), with additional signal in the amniotic ectoderm (red arrowhead). Black box within the XPS designates region magnified within inset. **D:** Late Bud/Neural Plate (LB) stage. The majority of IFITM3-positive cells localized to the XPS (see description for 3C), with additional signal in the intraembryonic posterior primitive streak (ips), dorsal epiblast (black arrows outlined in red) and amniotic

ectoderm (red arrowheads). An occasional cell localized to the allantoic bud (black arrowhead). **E:** Early Headfold (EHF) stage. IFITM3 extended along the length of the ACD (~120 μm (Downs et al., 2009); highlighted by brackets) from the base of the allantois into the proximal midline. Some IFITM3-positive cells localized within the distal ACD (black arrowhead). IFITM3 also localized to the dorsal epiblast (red arrows outlined in black), IPS, and the latter's associated posterior visceral endoderm (ipve; black arrow). An occasional vesicle of the yolk sac extraembryonic visceral endoderm (xve) contained IFITM3 signal (red arrowhead outlined in black). **F:** 1-somite (-s) stage, transverse profiles from the same specimen, with ventral toward the top, and dorsal toward the bottom of each panel. IFITM3-positive cells clustered within the ACD ($F_{1\text{-}2}$, asterisk) along the proximal midline of the allantois, at 42 μm (F_1) and 6 μm (F_2) above the base of the allantois. Some IFITM3-positive cells also localized to the allantois PVE (apve; black arrowhead in F_2). In the IPS, 12 μm below the base of the allantois (F_3), IFITM3-positive cells were dispersed along the dorsal-ventral axis. Black arrowheads highlight IFITM3-positive cells in the IPS-associated PVE (ipve). **G:** 5-s stage. IFITM3 extended from the proximal midline of the allantois to the IPS. Some IFITM3-positive cells in the allantois were closely associated with the nascent vessel of confluence (asterisk; Daane and Downs, 2011). Additional IFITM3 signal was observed in the amniotic ectoderm (outlined in black, magnified within inset) and the nascent hindgut (hg). **H:** 7-s stage. IFITM3 localized as a cytoplasmic spot with or without plasma membrane staining to the hindgut (e.g., black arrow outlined in red). Additional IFITM3-positive cells localized to the allantois (red arrow outlined in black). **I:** 10-s stage. Panel oriented with dorsal toward the top and ventral toward the bottom. IFITM3-positive cells localized to the ventral hindgut. IFITM3 also localized to the apical surface of some posterior surface ectoderm (black arrow). **J:** 14-s stage. Panel oriented with dorsal toward the top and ventral toward the bottom. IFITM3 localized to the ventral hindgut but also to somatopleure-associated mesoderm (red arrowheads), where it was found as cytoplasmic spots with plasma membrane staining. Additional IFITM3 localized to the apical surface of the VER (black arrowhead). **K:** 11-s stage. IFITM3 localized to the allantois (red arrow outlined in black) and VER (black arrowhead). Panel is a magnification of the area highlighted within the inset. Scale bar in A_2: 25.0 μm (A, C-E, G, H, K); 11.5 μm (A_1 inset); 11.2 μm (A_2 inset); 33.3 μm (B); 6.5 μm (C inset); 30.7 μm (F); 7.9 μm (G inset); 32.1 μm (I); 31.8 μm (J); 118.5 μm (K inset).

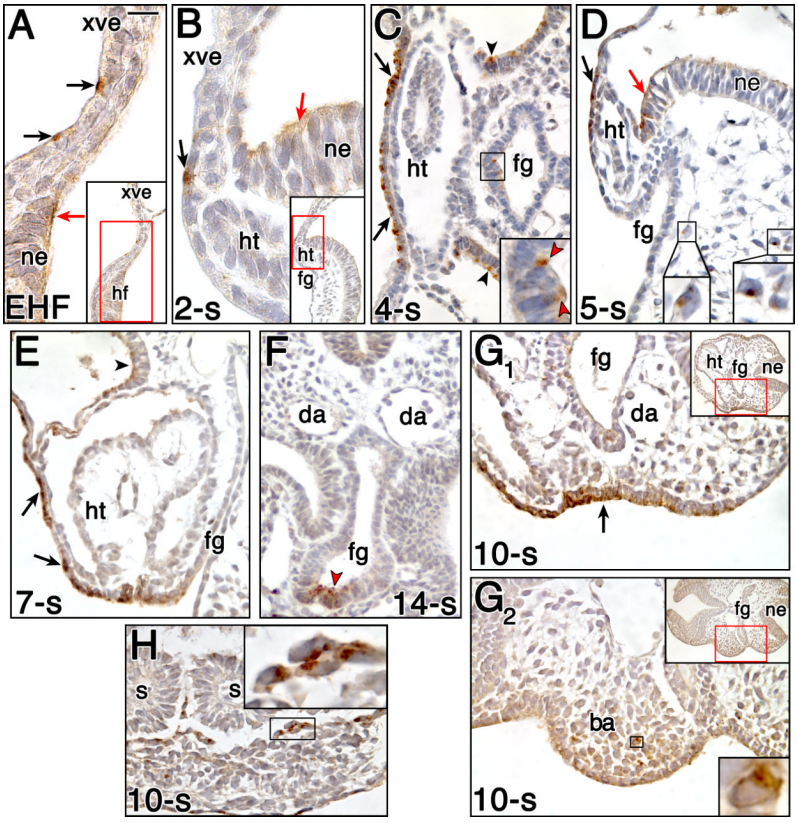

Fig. 4. IFITM3 localization to the anterior region (EHF-14-s stages; ~E7.75-9.0)

A: EHF stage. Large panel is a magnification of area boxed within inset. IFITM3 localized to the apical surface of some endoderm at the embryonic-extraembryonic junction of the anterior embryo (black arrows) and to the apical surface of the anterior-most neurectoderm (ne; red arrow) of the headfolds (hf). **B:** 2-s stage. Large panel is a magnification of area boxed within inset. IFITM3 continued to localize to the apical surface of some anterior embryonic endoderm (black arrow) near the extraembryonic visceral endoderm (xve) and anterior-most neurectoderm (red arrow). **C:** 4-s stage. IFITM3 localized to the apical surface of the majority of endoderm overlying the heart (ht; black arrows), anterior surface ectoderm (black arrowheads), and foregut (fg; highlighted by black box in larger panel and magnified within inset, with red arrowheads). **D:** 5-s stage. IFITM3 continued to localize to the apical surface of the endoderm overlying the heart (black arrow) and some neurectoderm (red arrow). In addition, IFITM3 localized as a cytoplasmic spot to some anterior mesenchymal cells (highlighted by black boxes in larger panel and magnified within insets). **E:** 7-s stage. IFITM3 localized to the apical surface of endoderm overlying the heart (black arrows), endoderm at the foregut opening, and surface ectoderm (black arrowhead). **F:** 14-s stage. IFITM3 persisted in the apical surface of the ventral foregut (red arrowhead outlined in black). **G:** 10-s stage. Large panels are magnifications of boxed areas within upper right insets. IFITM3 localized to the apical surface of anterior surface ectoderm posterior to (G_1; black arrow), but not overlying (G_2), the branchial arches (ba). IFITM3 localized as a cytoplasmic spot to some mesenchymal cells within the branchial arches (highlighted by black box in larger panel and magnified within lower right panel). **H:** 10-s stage. IFITM3 localized as a cytoplasmic spot to some lateral mesoderm adjacent to the somites (s). Area highlighted by black box is magnified within inset. Other abbreviations: da, dorsal aortae. Scale bar in A: 10 μm (A, B); 39.7 μm (A inset); 62.2 μm (B inset); 25.0 μm (C-E, G, H);

8.5 μm (C inset); 10.8 μm (D left inset); 11.3 μm (D right inset); 30.1 μm (F); 113.0 μm (G_1 inset); 124.4 μm (G_2 upper inset); 4.5 μm (G_2 lower inset); 8.0 μm (H inset).

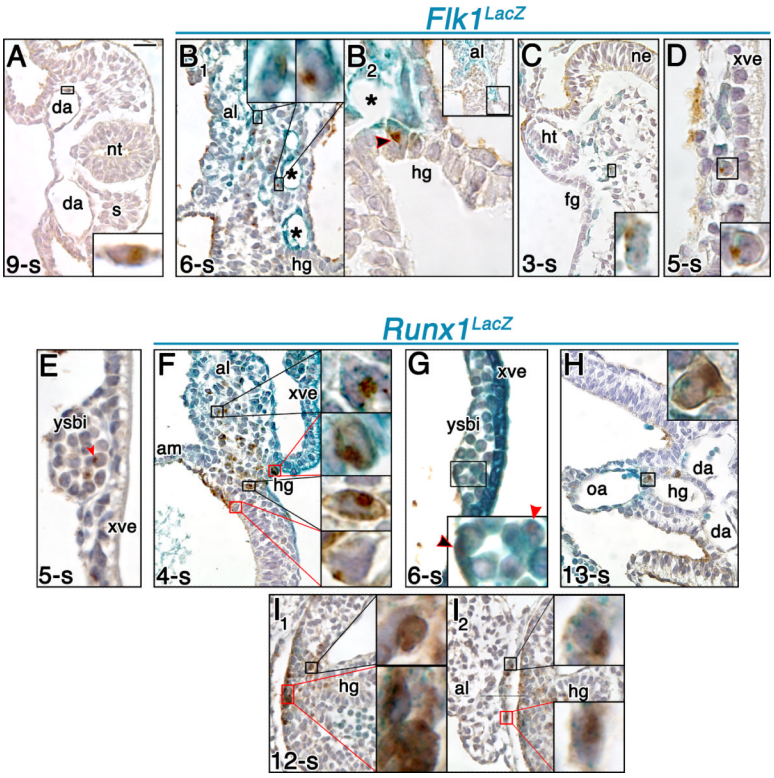

Fig. 5. IFITM3 co-localizes with *Flk1*^{LacZ} and *Runx1*^{LacZ}-expressing cells

Panels A, H, and I are of transverse sections with dorsal on the right and ventral on the left; all other panels are sagittal orientations, with anterior on the left and posterior on the right. Blue lines above the panels indicate *Flk1*^{LacZ} and *Runx1*^{LacZ} reporters. **A:** 9-s. IFITM3 localized as a cytoplasmic spot to an endothelial cell in the posterior dorsal aortae (da). Area highlighted by black box is magnified within inset. **B:** 6-s. IFITM3 co-localized with *Flk1*^{LacZ} expression in the allantois (al; B_1; exemplary cells boxed and magnified within insets) and the hindgut (hg; arrowhead in B_2; large panel is a magnification of area boxed within inset). Within the allantois (B_1 left inset) and hindgut (B_2), some IFITM3-positive *Flk1*^{LacZ}-expressing cells were closely associated with the vessel of confluence (asterisk). Note that the vessel of confluence is a continuous vessel that appears discontinuous in panel B_1 (asterisks) due to plane of section artifacts. **C:** 3-s. IFITM3 co-localized with *Flk1*^{LacZ} expression in the loose mesenchyme of the anterior embryo (boxed within larger panel and magnified within inset). **D:** 5-s. IFITM3 co-localized with *Flk1*^{LacZ} expression in hematopoietic cells within yolk sac blood islands (boxed within larger panel and magnified within inset). **E:** 5-s. IFITM3 localized as a cytoplasmic spot within some hematopoietic cells within the yolk sac blood islands (ysbi; red arrowhead). **F:** 4-s. IFITM3 co-localized with *Runx1*^{LacZ} expression in the posterior region, with exemplary cells boxed and magnified within insets, from top to bottom, from the allantois, hindgut endoderm, IPS, and dorsal epiblast. **G:** 6-s. IFITM3 co-localized with *Runx1*^{LacZ} expression in endothelial cells (black arrowhead outlined in red) and hematopoietic cells (red arrowhead) in yolk sac blood islands. Boxed area in larger panel is magnified within inset. **H:** 13-s. IFITM3 co-localized with *Runx1*^{LacZ} expression in some ventral hindgut cells (boxed in larger panel and magnified within inset). **I:** 12-s. IFITM3 co-localized with *Runx1*^{LacZ} expression in the VER (I_1) and the ventral cuboidal mesothelium of the allantois (I_2). Boxed regions within larger panel are magnified within insets. Other abbreviations: am, amnion; fg, foregut; ht, heart; ne, neurectoderm; nt, neural tube; oa, omphalomesenteric artery; s, somite; xve,

extraembryonic visceral endoderm. Scale bar in A: 25.0 μm (A, B_1, C, F, H, I); 4.4 μm (insets in A, B1, C, D, F); 7.8 μm (B2); 56.7 μm (B2 inset); 10.4 μm (D); 11.8 μm (E); 13.9 μm (G); 5.1 μm (G inset); 4.5 μm (H inset); 4.3 μm (I insets).

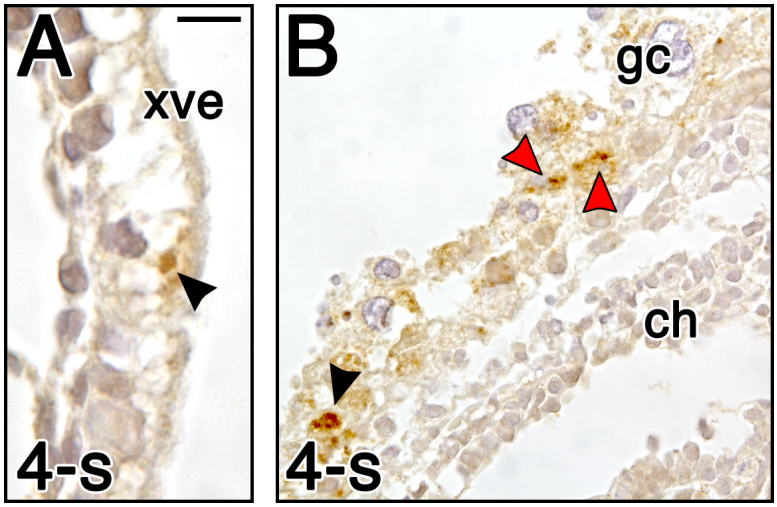

Fig. 6. IFITM3 localization to extraembryonic tissues outside of the posterior region

A: 4-s stage. IFITM3 localized to the vesicles of some yolk sac extraembryonic visceral endoderm (xve; arrowhead). **B:** 4-s stage. IFITM3 localized to cytoplasm of trophoblast giant cells (gc), where the staining ranged from small dark spots (red arrowheads) to broader cytoplasmic staining (black arrowhead). Other abbreviations: ch, chorion. Scale bar in A: 9.3 μm (A); 25.0 μm (B).

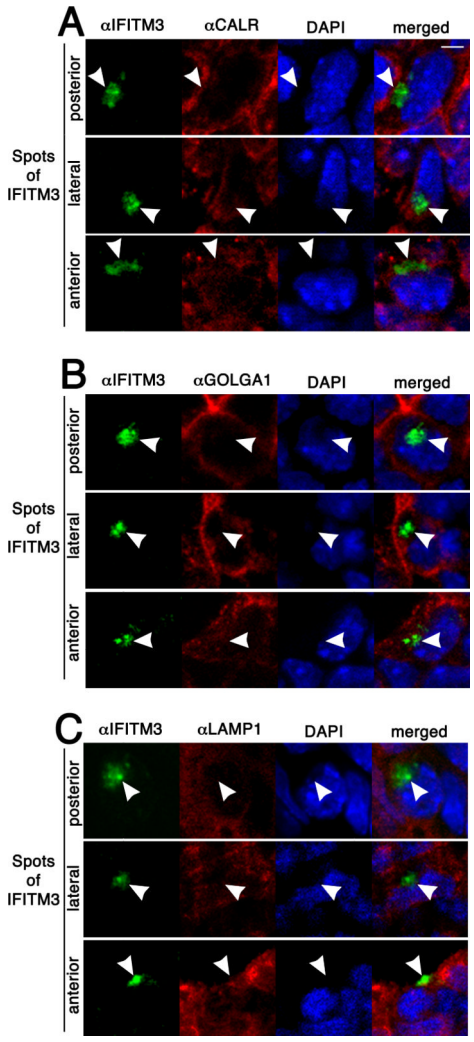

Fig. 7. Subcellular localization of the IFITM3 spot

Immunofluorescent colocalization of IFITM3 spots (white arrowheads) with organelle markers CALR (ER; **A**), GOLGA1 (Golgi apparatus; **B**), and LAMP1 (endolysomes; **C**). Specimens were counterstained for DNA with DAPI. Colocalization was not observed between these organelle markers and IFITM3 spots in the posterior, lateral, and anterior regions. This was confirmed via Pearson correlation coefficient reported in Table 3. Scale bar in upper right panel of A: 2.1 μm (A-C).

Table 1

Co-localization of IFITM3 protein with *Flk1*^{LacZ} expression at 3-6-s (~E8.25-8.5)

Tissue	Number of specimens exhibiting *Flk1*^{LacZ}/IFITM3 co-localization/total examined[a]
Allantois	5/5
Allantois/IPS-associated PVE/hindgut	3/5[b]
Anterior mesenchyme	4/5
Visceral yolk sac hematopoietic cells	5/5
Foregut	1/5
Lateral mesoderm	1/5
IPS	1/5

[a] A total of 5 LacZ-positive specimens was analyzed.

[b] All co-localizing cells were identified in the hindgut.

Table 2

Co-localization of IFITM3 protein with *Runx1*^{LacZ} expression at 2-6-s (~E8.25-8.5) and at 8-13-s (~E8.5-9.0)

Stage	Tissue	Number of specimens exhibiting *Runx1*^{LacZ}/IFITM3 co-localization/total examined[a]
2-6-s	Allantois	6/6
	IPS	5/6
	Posterior dorsal epiblast	5/6
	Amnion adjacent to posterior region	6/6
	Allantois/IPS-associated PVE/hindgut	6/6
	Anterior endoderm overlying heart	6/6
	Yolk sac hematopoietic cells	6/6
	VCM-associated yolk sac	3/6
	Anterior neurectoderm	3/6
	Anterior mesenchyme	1/6
8-13-s	VER	4/4[b]
	Allantois	7/7
	Hindgut	7/7
	Endothelial cells	7/7[c]
	Yolk sac hematopoietic cells	7/7
	Anterior endoderm overlying the heart	6/7
	Foregut	4/7
	Posterior surface ectoderm	2/7

[a] A total of 6 and 7 *LacZ*-positive specimens was examined at 2-6-s and 8-13-s, respectively.

[b] The VER was present in only 4/7 specimens examined.

[c] 7/7 specimens exhibited co-localization in endothelium of the yolk sac; 6/7 in omphalomesenteric artery; and 1/7 in posterior dorsal aortae.

Table 3

Colocalization of IFITM3 spots with organelle markers at 4-6-s (~E8.25-8.5)

Organelle	Associated marker	Localization of IFITM3 spots	No. spots analyzed	Pearson correlation coefficient (PCC)		
				Average (95% CI)	Minimum	Maximum
Endoplasmic reticulum (ER)	CALR	Posterior	48	-0.18 (±0.04)	-0.44	0.07
		Lateral	19	-0.09 (±0.07)	-0.33	0.24
		Anterior	46	-0.07 (±0.05)	-0.42	0.39
Golgi apparatus	GOLGA1	Posterior	69	-0.04 (±0.04)	-0.43	0.30
		Lateral	22	0.00 (±0.10)	-0.40	0.45
		Anterior	84	0.04 (±0.05)	-0.38	0.79[a]
Endolysosomes	LAMP1	Posterior	120	-0.09 (±0.02)	-0.45	0.29
		Lateral	26	-0.11 (±0.06)	-0.53	0.18
		Anterior	44	-0.08 (±0.04)	-0.52	0.15

IFITM3 was colocalized with each organelle marker in three specimens.

Abbreviations: CI, confidence interval; No., number.

[a]Only 3 of 84 anterior spots exhibited colocalization with GOLGA1 (PCC>0.5).